



# Mutations of Rad6 E2 ubiquitin-conjugating enzymes at alanine-126 in helix-3 affect ubiquitination activity and decrease enzyme stability

Received for publication, April 2, 2022, and in revised form, September 16, 2022. Published, Papers in Press, September 23, 2022.

<https://doi.org/10.1016/j.jbc.2022.102524>

Prakash K. Shukla<sup>1</sup>, Dhiraj Sinha<sup>2</sup>, Andrew M. Leng<sup>1</sup>, Jesse E. Bissell<sup>1</sup>, Shravya Thatipamula<sup>1</sup>, Rajarshi Ganguly<sup>1</sup>, Kaitlin S. Radmall<sup>1</sup>, Jack J. Skalicky<sup>3</sup>, Dennis C. Shrive<sup>1</sup>, and Mahesh B. Chandrasekharan<sup>1,\*</sup>

From the <sup>1</sup>Department of Radiation Oncology and Huntsman Cancer Institute, University of Utah School of Medicine, Salt Lake City, Utah, USA; <sup>2</sup>IHU, Aix Marseille University, Marseille, France; <sup>3</sup>Department of Biochemistry, University of Utah School of Medicine, Salt Lake City, Utah, USA

Edited by Brian Strahl

Rad6, an E2 ubiquitin-conjugating enzyme conserved from yeast to humans, functions in transcription, genome maintenance, and proteostasis. The contributions of many conserved secondary structures of Rad6 and its human homologs UBE2A and UBE2B to their biological functions are not understood. A mutant *RAD6* allele with a missense substitution at alanine-126 (A126) of helix-3 that causes defects in telomeric gene silencing, DNA repair, and protein degradation was reported over 2 decades ago. Here, using a combination of genetics, biochemical, biophysical, and computational approaches, we discovered that helix-3 A126 mutations compromise the ability of Rad6 to ubiquitinate target proteins without disrupting interactions with partner E3 ubiquitin-ligases that are required for their various biological functions *in vivo*. Explaining the defective *in vitro* or *in vivo* ubiquitination activities, molecular dynamics simulations and NMR showed that helix-3 A126 mutations cause local disorder of the catalytic pocket of Rad6 in addition to disorganizing the global structure of the protein to decrease its stability *in vivo*. We also show that helix-3 A126 mutations deform the structures of UBE2A and UBE2B, the human Rad6 homologs, and compromise the *in vitro* ubiquitination activity and folding of UBE2B. Providing insights into their ubiquitination defects, we determined helix-3 A126 mutations impair the initial ubiquitin charging and the final discharging steps during substrate ubiquitination by Rad6. In summary, our studies reveal that the conserved helix-3 is a crucial structural constituent that controls the organization of catalytic pockets, enzymatic activities, and biological functions of the Rad6-family E2 ubiquitin-conjugating enzymes.

Ubiquitination, the covalent posttranslational modification of proteins by the highly conserved 76 amino-acid protein ubiquitin (Ub), controls many aspects of cellular function (1, 2). Ubiquitination is a three-step process: first, an E1 ubiquitin-activating enzyme uses ATP to activate ubiquitin. Second, the E1 ubiquitin-activating enzyme attaches the

ubiquitin onto the active-site cysteine of an E2 ubiquitin-conjugating enzyme (henceforth referred to as an E2 enzyme) (1, 3). Third, an E3 ubiquitin-ligase (henceforth referred to as E3 ligase) and the ubiquitin-charged E2 enzyme target a substrate protein to catalyze the formation of an isopeptide bond between the C-terminus of ubiquitin and a nucleophile, which is typically a lysine side chain on the substrate protein (4). Monoubiquitination or addition of just one ubiquitin moiety is important during transcription and DNA repair (5–7). Ubiquitin contains seven lysine residues, which are targeted for cycles of ubiquitin addition to form polyubiquitin chains. Polyubiquitination through ubiquitin lysine-48 (K48) generally targets proteins for proteasomal degradation, whereas K63-linked ubiquitin chains regulate signal transduction and endocytosis (1, 8). Misregulation of ubiquitination is associated with numerous diseases ranging from neurological disorders to cancers (9–14).

E2 enzymes are central players in protein ubiquitination (15, 16). Humans express ~35 and *Saccharomyces cerevisiae* or budding yeast expresses 12 E2 enzymes. The E2 enzymes contain a distinctive core catalytic domain of about 150 amino acids called the UBC fold (17), which is comprised of four  $\alpha$ -helices, four  $\beta$ -sheets (also called a  $\beta$ -meander), and a conserved active-site cysteine (18). Additional residues also have roles in the catalytic functions of E2 enzymes: one is a conserved asparagine in a ‘flap’ or loop region present close to the active-site cysteine, which is part of the H x N triad that is proposed to aid in localizing the target lysine (19) or the active site (20) and in stabilizing the oxyanion formed in the reaction intermediate during the nucleophilic attack (21). Another is the “gateway residue”, which is a conserved serine or aspartate present in a loop that forms the opening of the E2 active-site cleft and implicated in the regulation of E2 activity (15, 22). Some E2 enzymes also contain internal and/or N- or C-terminal extensions to the UBC fold that have regulatory functions (14).

Functions for various secondary structures within the UBC domain of E2 enzymes have also been reported (15, 23): the N-terminal helix-1 in some E2s is an E1- or E3-binding surface. Loops in the front face close to the catalytic pocket of E2s

\* For correspondence: Mahesh B. Chandrasekharan, [mahesh.chandrasekharan@hci.utah.edu](mailto:mahesh.chandrasekharan@hci.utah.edu).

## Alanine-126 mutations in Rad6-family E2 enzymes

are functionally important in binding the RING domain of E3 ligases. The vast majority of the noncovalent interactions of E2 enzymes with ubiquitin, partner E3 ubiquitin-ligases, or other regulatory factors involve a so-called “backside” surface that is located on the face opposite from the catalytic pocket and made up of residues of the four  $\beta$ -sheets, the C-terminal end of helix-1, the intervening loops, and the C-terminal end of helix-4 (23–27). Despite these many structure-function studies, the roles for other regions within E2 enzymes, such as helix-3, remain not known.

Rad6 (Radiation sensitive 6) is an E2 enzyme in budding yeast that has well-established functions in transcription, DNA repair, and protein homeostasis that are accomplished through its interactions with different partner E3 ligases (Fig. 1A): Rad6

interacts with the Rad18 E3 ligase to monoubiquitinate PCNA and activate translesion DNA repair following DNA damage (28, 29). During transcription and other nuclear processes, Rad6 interacts with the Bre1 E3 ligase and the adapter protein Lge1 to monoubiquitinate histone H2B at K123 (H2BK123) (30–33), which in turn participates in the *trans*-histone regulation of methylation of histone H3 at K4 and K79 (34–37). Rad6 partners with the E3 ligase Ubr2 and the adapter protein Mub1 to polyubiquitinate phosphorylated Sml1, a ribonucleotide reductase inhibitor, resulting in its proteasomal degradation upon recovery from DNA damage (38). The Rad6-Ubr2 E2-E3 complex is also reported to regulate Rpn4 and Dsn1 protein levels *via* ubiquitination (39, 40). In the N-end rule pathway of targeted proteolysis, Rad6 and the Ubr1 E3 ligase

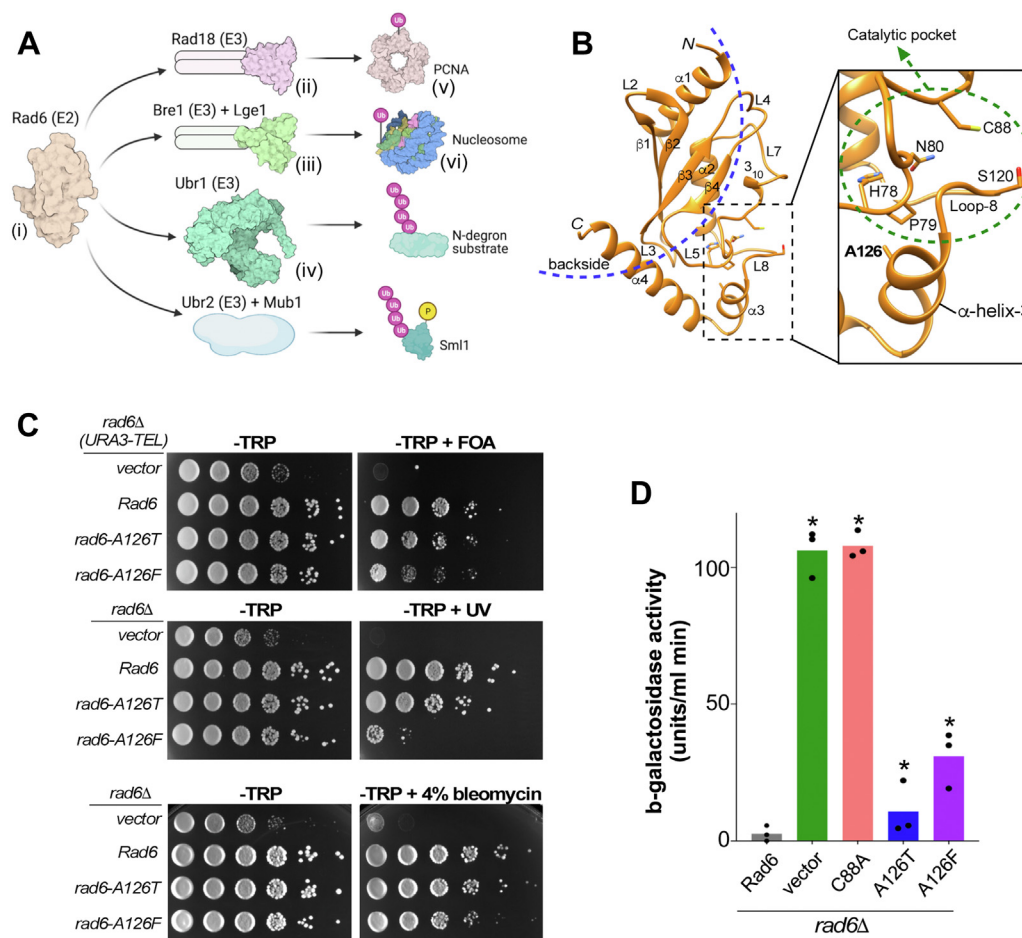


**Figure 1. Rad6 A126 mutations cause defects in telomeric gene silencing, DNA repair, and protein degradation in yeast.** A, illustration shows Rad6 and its partner E3 ubiquitin-ligases (Rad18, Bre1, Ubr1, or Ubr2) involved in mono- or poly-ubiquitination of the indicated target proteins. Crystal structure data were used in depictions of *i*, Rad6 (PDB ID: 1AYZ), *ii*, the Rad18 RING domains (PDB ID: 2Y43), *iii*, the Bre1 RING domains (PDB ID: 4R7E), *iv*, Ubr1 (PDB ID: 7MEX), *v*, PCNA (PDB ID: 6D0R), and *vi*, yeast nucleosome (PDB ID: 11D3). B, ribbon representation of Rad6. Secondary structures including  $\alpha$ -helices,  $3_{10}$ -helix,  $\beta$ -sheets, and intervening loops (L) are labeled. The region to the left of the blue dotted arc is the backside region of Rad6 comprised of residues in the  $\beta$ -sheets, intervening loops, and in the C-terminal ends of helices 1 and 4. Zoomed image shows the location of A126 in helix-3 and its spatial proximity to the catalytic pocket (encircled by green dotted line), which is comprised of the HPN motif, active-site C88, and the gateway residue S120 in loop-8. C, top panel, growth assay for telomeric gene silencing was conducted by spotting ten-fold serial dilutions of indicated strains on synthetic medium lacking tryptophan (-TRP) or containing 5-fluorooroic acid (-TRP+FOA). Middle panel, growth assay conducted by spotting a ten-fold serial dilution of the indicated strains on medium containing tryptophan with or without exposure to UV light. Bottom panel, growth assay was conducted by spotting a ten-fold serial dilution of the indicated strains on medium containing tryptophan with or without 4% bleomycin. D,  $\beta$ -galactosidase activity was measured in extracts of *rad6 $\Delta$  strains cotransformed with the plasmid for expression of N-end rule degradation reporter (R- $\beta$ -gal) and empty vector or constructs to express WT Rad6 or indicated mutants. Absence of Rad6 (*rad6 $\Delta$ ) or its activity (*rad6*-C88A) stabilizes the reporter yielding high  $\beta$ -gal activity or 100% degradation defect. In contrast, complete degradation of the reporter occurs in the presence of WT Rad6 or zero degradation defect. Plot shows values from three replicate assays. Asterisk, *p*-value < 0.05, statistical significance for  $\beta$ -gal activity in the indicated mutants relative to control WT Rad6 were computed using Student's *t* test. P, phosphate; Rad6, Radiation sensitive 6; Ub, ubiquitin.**

polyubiquitinate various proteins to target them for degradation by the proteasome machinery (41–43).

Structure-function studies have revealed that the N-terminal nine residues of helix-1 and amino acids 150 to 153 of Rad6 are necessary for its interaction with the Ubr1 E3 ligase (44). Residues 141 to 149 at the C-terminus and residues 10 to 22 at the N-terminus of Rad6 are necessary for binding to the Rad18 E3 ligase (45). A non-RING domain N-terminal region (amino acids 1–210) of the Bre1 E3 ligase binds the backside of Rad6 (46, 47). Rad6 possess a 23 amino-acid acidic tail that is important for its enzymatic activity *in vitro* and *in vivo* (48–50). Phosphorylation of gateway residue serine-120 (S120) of Rad6 occurs *in vivo* and regulates mono-ubiquitination of H2BK123 (51). Based on the studies on Rad6 and other E2 enzymes (18, 19, 21, 51, 52), the active-site C88, S120 in the active-site cleft or gate, and H78 and N80 in the HPN motif together constitute the catalytic pocket of Rad6 (Fig. 1B). Low-affinity noncovalent interactions of ubiquitin with the backside of Rad6 were reported to influence its processivity (24). Collectively, these studies have defined the role(s) of various residues and secondary structures within Rad6 to its protein–protein interactions and enzymatic functions; however, the contributions of other regions of the UBC domain to overall structure and enzymatic functions are not fully understood.

Nearly 2 decades ago, Liebman et al. reported the isolation and initial characterization of a missense threonine substitution at alanine (A) 126 in helix-3 of yeast Rad6. This mutant was defective in telomeric gene silencing and other functions of Rad6 (53). Here, using a multidisciplinary approach, we examined the contributions of A126 in helix-3 to the biological functions of Rad6. Mutations at A126 adversely affected the Rad6-mediated monoubiquitination and polyubiquitination of substrate proteins that regulate telomeric gene silencing, DNA repair, and protein degradation. Using molecular dynamics (MD) simulations and NMR, we show that mutations in A126 cause disorganization of local structure of the catalytic pockets as well as global structure of Rad6 that inhibit enzymatic activity and/or compromise protein stability in an E3 ligase-independent fashion. Our investigations further show that A126 mutation(s) in helix-3 also disrupt the structure and enzymatic activity of human Rad6 homologs. Overall, our studies reveal that the conserved helix-3 is a crucial structural constituent of yeast and human Rad6 E2 ubiquitin-conjugating enzymes.

## Results

### **A126 mutations disrupt telomeric gene silencing, DNA repair, and protein degradation functions of Rad6**

A screen for *RAD6* alleles that cause defects in telomeric gene silencing identified a mutant with a threonine substitution at A126 of Rad6 (53). The *rad6-A126T* allele also conferred sensitivity to UV irradiation, indicating impaired DNA repair function, and was also shown to be defective in N-end rule protein degradation (53). A126 is in helix-3 of

Rad6, close to the catalytic pocket (Fig. 1B). To investigate how mutations in A126 residue influence the biological functions of Rad6 in telomeric gene silencing, DNA repair, and protein degradation, we created yeast constructs for expression of the *rad6-A126T* mutant and of a Rad6 protein with a bulkier phenylalanine (F) substitution (*rad6-A126F*).

To test the effect of these mutations on telomeric gene silencing, we transformed the constructs into a *rad6* null mutant yeast strain (*rad6Δ*) that harbors a silencing reporter gene (*URA3*) integrated near the left end of chromosome VII. As controls, either the empty vector or a plasmid for the expression of WT Rad6 was transformed into this reporter strain. Transcriptional repression of the telomere-proximal *URA3* reporter occurred in the presence of WT Rad6, which allowed yeast cells to survive on a media containing the counterselection agent 5-fluoroorotic acid (5FOA) (54), whereas the absence of Rad6 resulted in the transcriptional activation and production of the *URA3* enzyme, which converts 5FOA to toxic 5-fluorouracil, inhibiting growth (Fig. 1C, top panels). Consistent with the previous report (53), expression of the *rad6-A126T* mutant resulted in slower growth on 5FOA medium than the control strain that expressed WT Rad6 (Fig. 1C), indicating activation of the *URA3* reporter and a telomeric silencing defect. The *rad6-A126F* mutant showed a more drastic growth retardation on 5FOA medium than the *rad6-A126T* mutant strain (Fig. 1C), revealing that this mutation causes a severe telomeric gene silencing defect. Next, we examined the growth of Rad6 A126 mutant strains following exposure to DNA damaging agents: UV or the radiomimetic drug bleomycin (55). While the *rad6-A126T* mutant showed a subtle slow growth defect, the *rad6-A126F* mutant had a more severe growth retardation upon UV irradiation or bleomycin treatment than the control strain that expresses WT Rad6 (Fig. 1C, middle and lower panels). These results suggest that mutations in A126 residue impair the DNA repair functions of Rad6.

Proteins with N-terminal arginine are degraded by the N-end-rule pathway, where polyubiquitination by Rad6 precedes proteasome-mediated proteolysis (56). To measure the N-end rule activity, extracts were prepared for enzyme assays from strains expressing either WT or mutant Rad6 along with the reporter beta-galactosidase protein with arginine as the N-terminal amino acid (R-β-Gal) (57). Low or no activity was obtained for R-β-Gal in extracts prepared from the strain with WT Rad6 (Fig. 1D). In contrast, extracts prepared from strains lacking Rad6 (*rad6Δ*) or expressing the catalytic-dead mutant (*rad6-C88A*) yielded very high activity compared to the control strain with WT Rad6 (Fig. 1D), indicating stabilization of R-β-Gal levels and a defect in the N-end-rule degradation. Extracts prepared from *rad6-A126T* and *rad6-A126F* mutant strains showed higher galactosidase activity than the control strain with WT Rad6 (Fig. 1D), indicating that these mutants are also defective in the N-end rule protein degradation process. Collectively, our results showed that mutations at A126 compromise Rad6's

## Alanine-126 mutations in Rad6-family E2 enzymes

functions in telomeric gene silencing, DNA repair, and targeted proteolysis.

### A126 mutations adversely affect Rad6-mediated monoubiquitination or polyubiquitination of substrate proteins in vivo

Next, we asked whether Rad6 A126 mutations disrupt ubiquitination of substrate proteins histone H2B and PCNA or Sml1, which are involved in telomeric gene silencing and DNA repair, respectively (28, 34, 38). A complex of Rad6, Bre1, and Lge1 catalyzes histone H2BK123 monoubiquitination (H2Bub1) (30–32), which regulates methylation (me) of histone H3K4 (34, 36). Decreased trimethylation of H3K4 (H3K4me3) causes telomeric gene silencing defect (37, 58, 59). Therefore, we measured the steady-state levels of H2Bub1 and H3K4me in *rad6-A126T* and *rad6-A126F* strains using immunoblotting. When expressed in the *rad6Δ* strain, both *rad6-A126T* and *rad6-A126F* mutants caused an apparent complete loss of H2Bub1 (Fig. 2A, lanes 3–4).

In yeast, steady-state H2Bub1 levels are a net result of two opposing enzymatic activities: Rad6-Bre1-Lge1-mediated ubiquitin conjugation and subsequent removal by deubiquitinases Ubp8 and Ubp10 (60, 61). To directly examine the effects of A126 mutations on histone H2B monoubiquitination, we measured the steady-state H2Bub1 levels upon expression of *rad6-A126T* and *rad6-A126F* mutants in a *rad6Δ* strain that additionally lacks Ubp8 and Ubp10 (*i.e.*, *ubp8Δ ubp10Δ rad6Δ*). In this background, the *rad6-A126T* mutant caused a 25% reduction in H2Bub1 levels, and the *rad6-A126F* mutant caused about 50% decrease when compared to the control strain with WT Rad6 (Fig. 2A, compare lanes 7–8 to lane 6). These results demonstrate that mutations at A126 compromise the ability of Rad6 to catalyze histone H2B monoubiquitination *in vivo*. Immunoblotting also revealed that the steady-state levels of H3K4me3 were decreased in *rad6-A126T* and *rad6-A126F* mutants when compared to the control strain (Fig. 2B), as expected given the reduced H2Bub1 levels and telomeric silencing defects observed in these mutants (Figs. 1C and 2A). Moreover, the observed decrease in the H2Bub1-dependent H3K4me3 levels matches with the degree of telomeric gene silencing defect displayed by the Rad6 A126 mutants.

Following DNA damage, Rad6 and Rad18 E3 ligase catalyze PCNA monoubiquitination (PCNAub1) (28) (Fig. 1A). H2BK123 deubiquitinase Ubp10 also removes the ubiquitin from PCNAub1 (62). We therefore examined PCNAub1 levels in the *rad6-A126T* and *rad6-A126F* mutants expressed in a *rad6Δ ubp10Δ* double-deletion strain after induction of DNA lesions using methyl methane sulfonate treatment. The *rad6-A126T* and *rad6-A126F* mutants had severe reductions in the DNA damage-induced PCNAub1 levels when compared to the control strain with WT Rad6 (Fig. 2C). After DNA damage, Sml1 is phosphorylated and then targeted for proteasomal degradation in a Rad6-Ubr2-Mub1-dependent

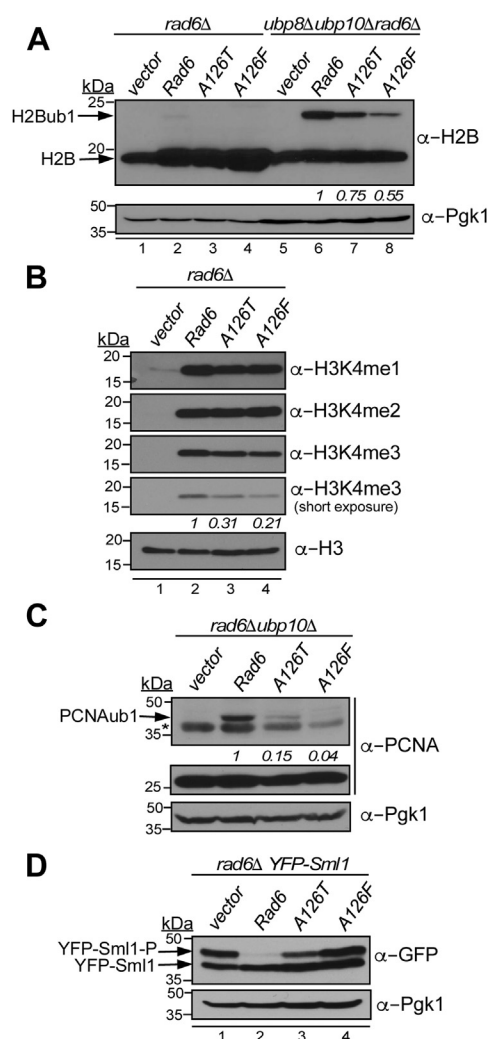


**Figure 2. Mutations in A126 of Rad6 impair its target protein ubiquitination functions *in vivo*.** A, immunoblot for H2Bub1 in a *rad6Δ* strain and in a strain that lacks Rad6, Ubp8, and Ubp10 transformed with empty vector or constructs to express WT Rad6 or the mutants *rad6-A126T* or *rad6-A126F*. Fold change in H2Bub1 levels in the A126 mutants relative to WT Rad6 (set as 1) in the triple mutant background are shown and were quantified by densitometry from two independent experiments. B, immunoblot for histone H3K4 methylation (mono, me1; di, me2; tri, me3) in extracts prepared from the *rad6Δ* strain that expresses the indicated proteins. Histone H3 levels served as loading control. H3K4me3 and H3 levels were quantified by densitometry from two independent experiments. H3K4me3 levels normalized to H3 levels in the mutants are shown relative to the strain that expresses WT Rad6 (set as 1). C, immunoblot for monoubiquitinated PCNA monoubiquitination (PCNAub1) in the *rad6Δ ubp10Δ* strain transformed with empty vector or constructs to express WT Rad6 or the indicated mutants and treated with 0.02% methyl methane sulfonate for 90 min. Pgk1 served as loading control. For each strain, PCNAub1 and Pgk1 levels were quantified by densitometry. PCNAub1 levels normalized to Pgk1 levels in a mutant are shown relative to that in a control strain expressing WT Rad6 (set as 1). They were obtained by averaging the values from two independent experiments. For quantitation shown in panels (A–C), *p*-value was <0.05. The asterisk indicates a cross-reacting protein. D, immunoblots for phosphorylated and unphosphorylated YFP-tagged Sml1 expressed in *rad6Δ* strain and transformed with empty vector or constructs to express WT Rad6 or the indicated mutants. Cultures were treated with 3 μg/ml bleomycin for 45 min, followed by recovery from DNA damage for 35 min in fresh medium without bleomycin. Pgk1 levels served as loading control. A representative immunoblot from two independent experiments is shown. In all panels, molecular weights of the protein standards used as size markers are indicated. Rad6, Radiation sensitive 6.

manner (38). Consistent with this reported study, we observed that the slow-migrating phosphorylated Sml1 was eliminated in the presence of Rad6 during the recovery phase after exposure to DNA damaging agent bleomycin, but it persisted in the absence of Rad6 (Fig. 2D, compare lanes 1–2). Phosphorylated Sml1 was retained in both rad6-A126T and rad6-A126F mutant strains upon recovery from DNA damage (Fig. 2D, lanes 3–4). Therefore, mutations in A126 compromise the ability of Rad6 to perform monoubiquitination or polyubiquitination of histone H2B, PCNA, Sml1, and likely other substrate proteins *in vivo*. While Rad6 A126 mutations do not appear to drastically perturb normal cellular growth (Fig. 1C, -TRP media), our results from immunoblotting studies together provide a molecular explanation for the observed defects in telomeric gene silencing and N-end rule degradation and impaired growth upon exposure to DNA damaging agents, seen in yeast cells with mutations in A126 of Rad6.

#### A126 mutations do not disrupt interactions of Rad6 with its partner E3 ubiquitin ligases

Ubiquitination of substrate proteins by Rad6 *in vivo* is accomplished *via* its partnership with different E3 ligases: Ubr1, Ubr2, Bre1, and Rad18 (Fig. 1A). To investigate whether defective substrate protein ubiquitination by Rad6 A126 mutants is due to disruption of the association with these partner E3 ligases, we examined the interactions of WT or mutant Rad6 with E3 ligases *in vitro* using copurification and within yeast cells by coimmunoprecipitation. Published studies have delineated amino acids 1 to 214 of Bre1 and 301 to 487 of Rad18 as the minimal Rad6-binding regions *in vitro* (45–47). Therefore, we coexpressed WT or mutant Rad6 tagged with hexahistidine (His<sub>6</sub>) along with these minimal Rad6-binding regions of Bre1 or Rad18 (Bre1R6BR or Rad18R6BR, respectively) in bacteria. Bacterial lysates prepared after coexpression were subjected to metal affinity purification to capture His<sub>6</sub>-tagged WT or mutant Rad6 and copurifying Bre1R6BR or Rad18R6BR, which were then evaluated by SDS-PAGE and Coomassie blue staining. The amounts of Bre1R6BR or Rad18R6BR that copurified with His<sub>6</sub>-rad6-A126T and His<sub>6</sub>-rad6-A126F were increased or were similar, respectively, to the amounts that copurified with control His<sub>6</sub>-Rad6 (Fig. S1, A and B).

For coimmunoprecipitation, we expressed Flag epitope-tagged WT or mutant Rad6 in a *rad6Δ* strain that also contained Myc-tagged Rad18, V5-tagged Ubr1, or HA-Ubr2, which enable their detection by immunoblotting. Immunoaffinity purification using anti-Flag antibody and subsequent immunoblotting showed that the levels of Ubr1, Ubr2, Rad18, and Bre1 that coprecipitated with rad6-A126T-Flag or rad6-A126F-Flag were similar to or slightly increased to their amounts that coprecipitated with WT Rad6-Flag (Fig. S1C). Taken together, these data from copurification and coimmunoprecipitation experiments showed that mutations in A126 do not abolish or diminish the interactions of Rad6 with its partner E3 ligases necessary for target protein ubiquitination

*in vivo*. Importantly, these results suggested that the A126 mutations in helix-3 could adversely affect the E3 ligase-independent enzymatic activity of Rad6.

#### A126 mutations adversely affect activity and stability of Rad6

To test this possibility, we next examined the *in vitro* ubiquitination activities of rad6-A126T and rad6-A126F mutants. WT Rad6, the catalytic-dead mutant rad6-C88A, rad6-A126T and rad6-A126F were expressed in and purified from bacteria. UBE2B or Rad6b, the human homolog of yeast Rad6, was reported to form ubiquitin chains in solution in the absence of an E3 ligase and a target protein (63). However, yeast Rad6 showed significantly compromised *in vitro* intrinsic ubiquitin chain formation activity when compared to its human homologs (Fig. S2). *In vitro* in the absence of E3 ligases, Rad6 was reported to nonspecifically polyubiquitinate histone proteins (49, 64). Consistent with these studies, robust polyubiquitination of histone H2B was observed with WT Rad6 in our *in vitro* system (Fig. 3A, lanes 2–4). Monoubiquitination was decreased, and polyubiquitination was nearly absent in the assay with the rad6-A126T mutant, and neither was detected in the rad6-A126F mutant similar to that in the catalytically inactive rad6-C88A mutant (Fig. 3A). Overall, mutations at A126 compromise the enzymatic activity of Rad6 to ubiquitinate substrate protein *in vitro*.

Next, we examined the effects of A126 mutations on levels of Rad6 *in vivo*. First, whole-cell lysates were prepared from strains expressing Flag epitope-tagged WT or mutant Rad6 and subjected to immunoblotting. The global or steady state levels of both rad6-A126T and rad6-A126F mutants were lower than that of WT Rad6 (Fig. 3B). To determine whether this decrease in the steady state levels was due to compromised protein stability, we expressed a Flag epitope-tagged WT or mutant Rad6 in yeast from a galactose-inducible promoter (*GALI*) and then added glucose to inhibit transcription as previously described (65). Protein levels were then measured at various time points using immunoblotting. The levels of rad6-A126T and rad6-A126F mutants were drastically reduced compared to WT Rad6 at 2 h after glucose-mediated transcription shut-off (Fig. 3C), indicating that mutations in A126 are detrimental to the stability of Rad6. We further tested whether the decreased stability of the mutants is due to proteasome-mediated proteolysis. Indeed, global levels of Rad6 as well as the rad6-A126T and rad6-A126F mutants were increased when cells were treated with the proteasomal inhibitor MG132 (66) (Fig. S3). Taken together, our results indicate that mutations in A126 compromise both activity and stability of Rad6.

#### A126 mutations alter the structure of Rad6

In the reported crystal structure of Rad6 (67), A126 is in close spatial proximity to the catalytic pocket composed of the active-site C88, residues in the HPN motif, and the gateway S120 (Figs. 1B and S4). These residues were shown to be necessary for or to regulate the activity of Rad6 (18, 51, 68) or E2 enzymes in general (15, 22, 23). We therefore postulated

## Alanine-126 mutations in Rad6-family E2 enzymes

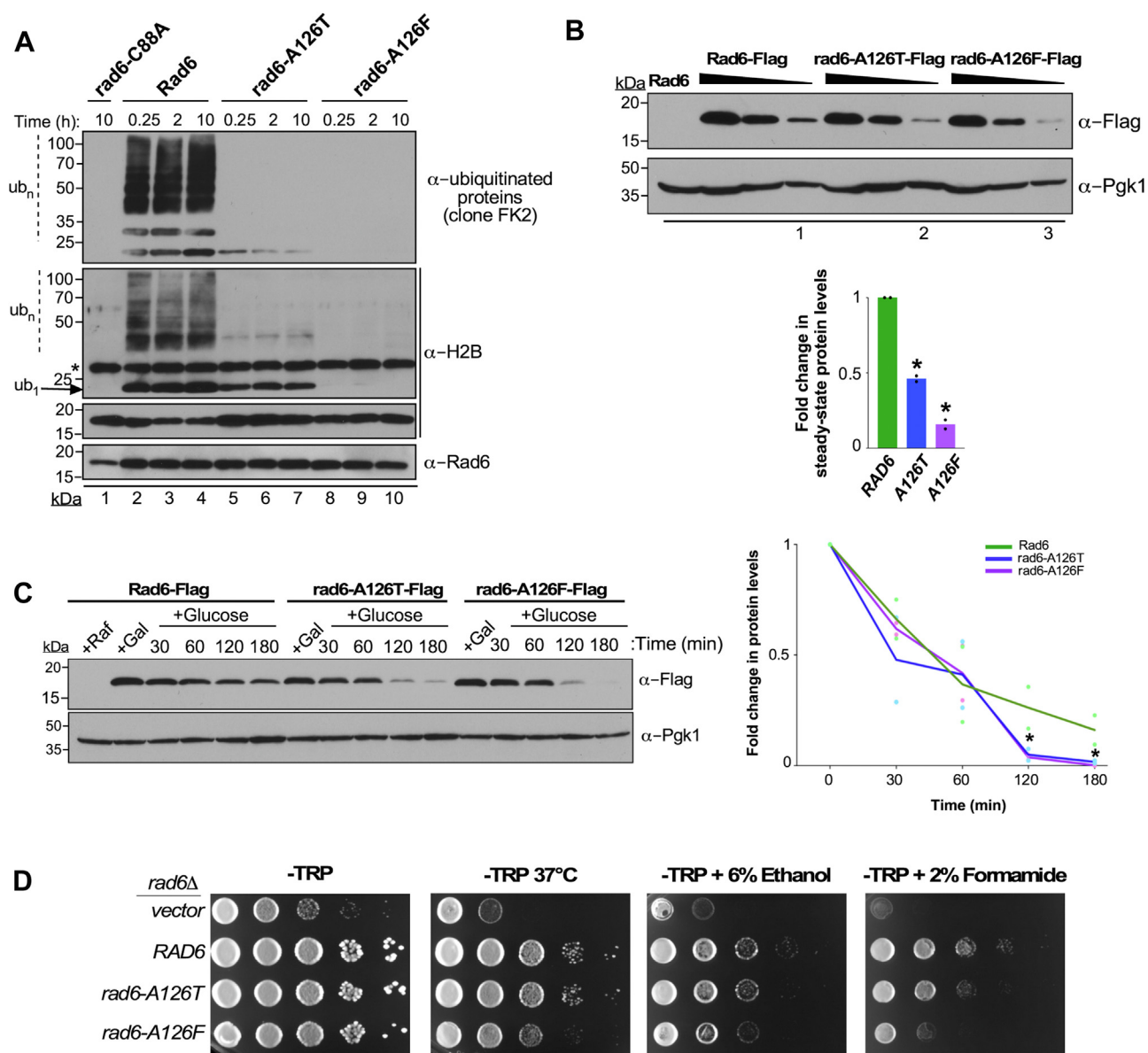


**Figure 3. A126 mutations disrupt enzymatic activity and stability of Rad6.** *A*, immunoblot of products of an *in vitro* ubiquitination assay with recombinant WT Rad6 or indicated mutants. Enzyme was incubated at 30 °C for the indicated time along with ubiquitin (Ub), Uba1, ATP/Mg<sup>2+</sup>, and yeast histone H2B (substrate). The reaction mix was then resolved by SDS-PAGE prior to immunoblotting. The asterisk indicates a cross-reacting protein. The catalytic-dead mutant rad6-C88A served as a control. *B*, *left*, immunoblot of Flag-tagged WT or mutant Rad6. A two-fold serial gradient of the extracts prepared from the indicated strains were resolved by SDS-PAGE prior to immunoblotting. Extract from the strain expressing Rad6 served as a 'no tag' control. *Right*, plot of mean fold-change in the steady-state levels of A126 mutant relative to WT Rad6 ( $\pm$  SEM from two independent experiments) based on densitometry quantitation, for which the signals in the numbered lanes were used. The signals for WT or mutant Rad6 were initially normalized to the signals for Pgk1, which serves as a loading control. *C*, *left*, immunoblot for analysis of stability of Flag epitope-tagged Rad6 or mutants grown in a medium containing raffinose (+Raf; uninduced) or galactose (+Gal; induced) and at different time points after transcription from the *GAL1* promoter was halted by adding glucose. Pgk1 served as loading control and for normalization. *Right*, plot shows densitometric values for WT or mutant Rad6 protein at different time points after glucose-mediated transcriptional inhibition relative to that in the induced state (+Gal, 0 min). Asterisk, *p*-value < 0.05 (Student's *t* test). *D*, growth assay was conducted by spotting ten-fold serial dilution of the indicated yeast strains on synthetic medium without tryptophan (-TRP) or in medium containing 6% ethanol or 2% formamide and incubated at 30 °C. Cells spotted on -TRP medium were also subjected to heat stress by incubation at 37 °C. Rad6, Radiation sensitive 6; Ub<sub>1</sub>, monoubiquitinated H2B; Ub<sub>n</sub>, polyubiquitinated H2B.

that the impaired protein ubiquitination or stability of the Rad6 A126 mutants might be due to the adverse effects of these mutations on the overall structure of Rad6.

Growth sensitivity of yeast mutants to high temperature (37 °C), ethanol, or formamide indicate general protein structural defects presumably from disrupted hydrogen bonds (69). Spotting assays showed that the rad6-A126T and

rad6-A126F mutants have reduced growth at 37 °C and in media containing 6% ethanol or 2% formamide when compared to the control strain expressing WT Rad6 (Fig. 3D), suggesting that mutations at A126 can alter the structure of Rad6.

To test this possibility, we first performed MD simulation, which allows one to evaluate structural details and dynamic

behaviors of proteins by measuring the trajectory of individual atoms over time (70–73). *In silico* models of rad6-A126T and rad6-A126F were created using the crystal structure data for native Rad6 (PDB ID: 1AYZ (67)). We then performed all-atom MD simulations for a period of 100 ns. In MD simulations, analysis of RMSD of the backbone or C $\alpha$  atoms provide an overall view of the changes occurring in a protein over the course of the simulation (74). In the RMSD plot, the rad6-A126T mutant showed deviations during the course of simulation, but both native Rad6 and the mutants showed very similar deviations at the end of simulation (Fig. S5A), suggesting that the A126 mutations do not alter the overall structural topology of Rad6.

To determine the impact of mutations on local flexibility and dynamic behavior of individual amino acids, we calculated root-mean-square fluctuation (RMSF) values for the backbone residues in native as well as mutant Rad6 (75–77). Both mutants had higher RMSF values, indicating higher flexibility than the native Rad6 at residues in the vicinity of T126 or F126 including those in helix-3 and in the adjoining loop-8 region (amino acids 114–S120) (Fig. 4A). Additional subtle increases or decreases in RMSF values were also observed for one or both mutants at multiple spatially close and distant residues including those near the catalytic C88 residue. These results suggest that mutation in A126 can either enhance or constrain the flexibility of individual residues to cause local conformational changes in Rad6.

To further test this possibility, we performed time-dependent secondary structure fluctuation analysis using definition of secondary structure of proteins (DSSP) (78), which can yield additional information on the structural flexibility of proteins. The DSSP plot for native Rad6 shows that many of its secondary structures are stable and remain unchanged during the course of MD simulation. However, certain secondary structures, such as helix-3, are flexible and are converted to a  $3_{10}$ -helix or turns during the simulation but revert to their original state at the end of the simulation (Fig. S5B). The DSSP plots for the two mutants show reorganization of the  $3_{10}$ -helix (residues 90–93) close to the active-site C88 into an  $\alpha$ -helix (Fig. S5B). Moreover, the helix-2 and helix-3 are reorganized into  $3_{10}$ -helix or turns in the rad6-A126F mutant (Fig. S5B). These findings indicate that mutations in A126 can alter the flexibility and/or conformations of the secondary structures within Rad6.

Given that secondary structure elements in proteins are stabilized by hydrogen bonding, we used the *hbond* tool to analyze the extent of hydrogen bonding in the native and mutant Rad6 proteins (79). The number of hydrogen bonds were reduced during the MD simulation in the rad6-A126F mutant compared to native Rad6, although the stability of rad6-A126T mutant was similar to that of WT Rad6 (Fig. S5C). Computational stability prediction using DynaMut 2.0 (80) further indicated that rad6-A126T and rad6-A126F are both destabilized relative to the native protein (Table S1). Taken together, these computational analyses indicated that mutations in A126 can alter the flexibility of individual residues and/or conformations of local secondary structures of Rad6, in

particular those within or near the catalytic pocket. Moreover, these observations match well with the general protein structural defects displayed by the rad6-A126T and rad6-A126F mutants in growth assays (Fig. 3D).

#### A126 mutations perturb the catalytically relevant residues of Rad6

To experimentally validate the data from MD simulations and to directly examine the structural changes caused by the Rad6 A126 mutations, we then employed NMR. We expressed and purified  $^{15}\text{N}$  isotope-labeled WT Rad6 and the mutants rad6-A126T or rad6-A126F from bacteria and recorded their two-dimensional  $^{15}\text{N}$ - $^1\text{H}$  heteronuclear single quantum coherence (HSQC) NMR spectra. Complete residue assignments were performed on the NMR spectra obtained for WT Rad6, and a published dataset was also used (24). The NMR spectrum for each mutant was then overlaid on the assigned NMR spectra for WT Rad6 (Fig. 4B). NMR chemical shifts are very sensitive to change in protein structure and dynamics and arise from small differences in the local magnetic field and shifts in equilibria. For a given residue, a perfect overlap of NMR signals between the mutant and WT Rad6 indicates no structural perturbation. On the other hand, partial or no overlap in NMR signals between a mutant and WT indicates a structural anomaly or a chemical shift perturbation caused by the introduced mutation. The HSQC plot showed no or poor overlap of NMR signals at multiple residues in the rad6-A126T and rad6-A126F mutants when compared with the signals in the WT Rad6 spectrum (Fig. 4B). Quantitation of chemical shift perturbations showed that A126 mutations alter the positions of residues in the helix-3 and in the adjacent helix-4 (Figs. S6 and 4C). Additional perturbations were also evident at distant sites on the backside of Rad6 that are implicated in noncovalent interactions with ubiquitin (24). Importantly, the A126 mutations caused perturbations in residues H78, N80, the active-site residue C88, and the gateway residue S120 (Fig. 4, B and C), which together constitute the catalytic pocket of Rad6. Thus, these NMR data confirmed the findings of MD simulations and demonstrate that mutations in A126 perturb the structure of Rad6, importantly at residues crucial for its enzymatic activity.

Overall, these results from MD simulations and NMR along with the growth phenotypes together demonstrate that mutations in helix-3 cause structural perturbations including at the catalytic pocket and thus provide an explanation for their adverse effects on enzymatic activity and overall protein stability of Rad6.

#### A126 mutations alter the structures of human Rad6 homologs UBE2A and UBE2B

The alanine at position 126 in helix-3 is evolutionarily conserved from yeast to humans (Fig. S4). Therefore, we then investigated the effects of A126T or A126F mutation on the structures of UBE2A and UBE2B, the human homologs of yeast Rad6. Computational stability prediction (80) indicated that A126T and A126F are both destabilizing mutations in

## Alanine-126 mutations in Rad6-family E2 enzymes

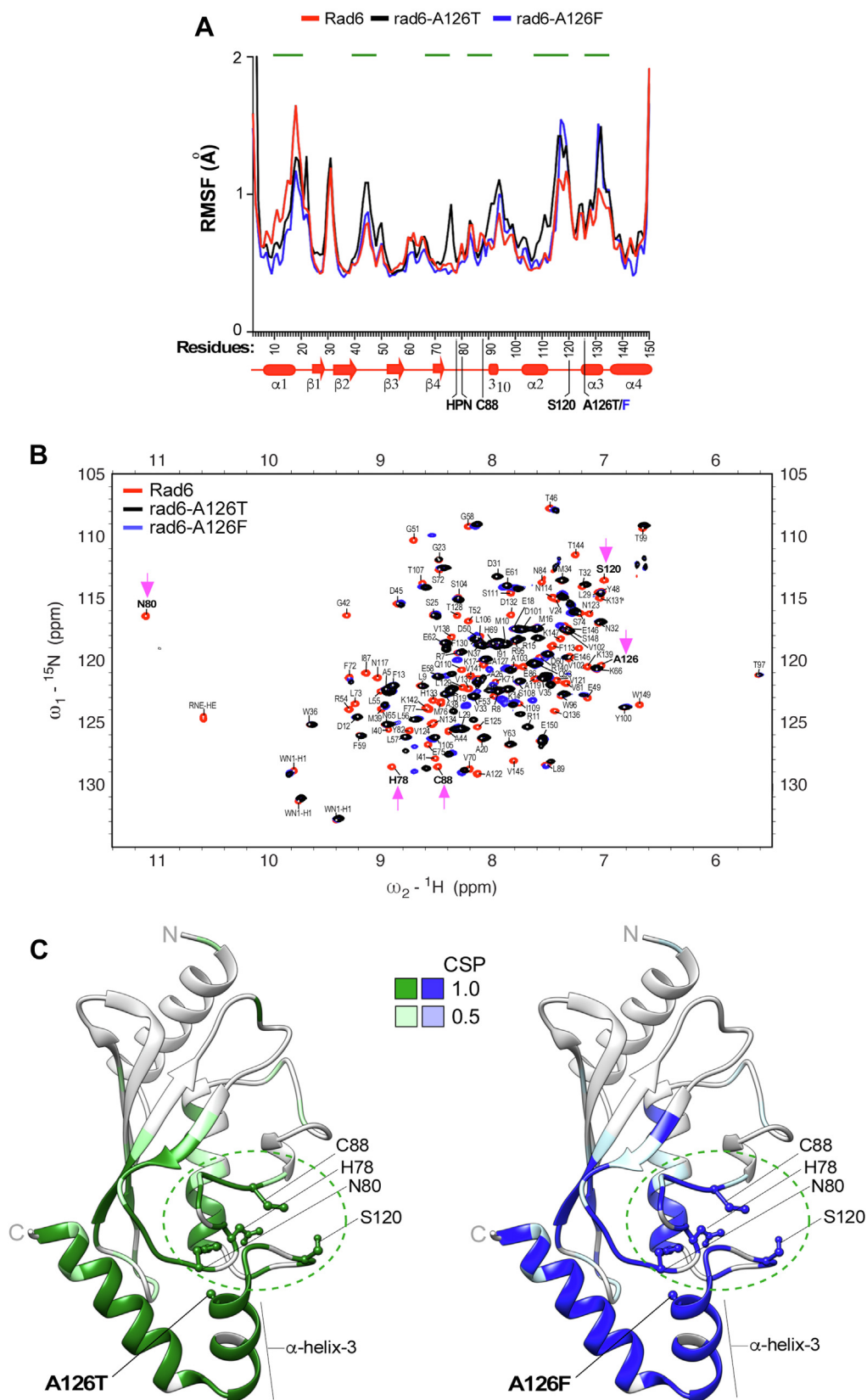


**Figure 4. A126 mutations disorganize local as well as global structure of Rad6.** *A*, RMSF analyses of Rad6 (red), rad6-A126T (black), and rad6-A126F (blue). Green lines indicate residues with increased or decreased RMSF values in a mutant relative to WT Rad6, indicative of enhanced or constrained flexibility, respectively. Schematic below the x-axis shows the secondary structures of Rad6. The site of mutation in  $\alpha$ -helix-3, the active-site C88, and other catalytically crucial amino acids of Rad6 are indicated. *B*, overlay of the  $^1\text{H}$ - $^{15}\text{N}$  HSQC spectra of rad6-A126T (black) and rad6-A126F (blue) mutant on the spectrum of Rad6 (red). Magenta arrows point to either a complete absence of NMR signal or a drastic chemical shift perturbation for the indicated residues of the catalytic pocket in the mutants compared to WT Rad6. *C*, chemical shift perturbations (CSPs) in the A126 mutant mapped onto the Rad6 crystal



UBE2A and UBE2B (Table S1). Next, we created *in silico* models for threonine or phenylalanine substitution at A126 using the reported crystal structures for UBE2A (PDB ID: 6CYO) (81) and UBE2B (PDB ID: 2YB6) (63) in order to examine their effects on protein structure and conformation using MD simulations.

MD simulations for the A126T mutation in UBE2A or UBE2B showed the following: RMSD plots for UBE2A-A126T and UBE2B-A126T mutants showed patterns of deviations very similar to those of their respective native proteins (Fig. S7A), indicating that threonine substitution at 126 does not cause gross changes in overall topologies of these human proteins. However, higher RMSF values, indicating increased flexibility, were observed for both UBE2A-A126T and UBE2B-A126T at residues near the introduced mutations in helix-3 including in the active-site cleft containing the gateway S120 residue when compared to their respective native proteins (Fig. 5A). Consistent with this increased local flexibility, DSSP plots showed disorganization of secondary structures, such as loop-8, which contains the gateway residue S120, and helix-4 in both UBE2A-A126T and UBE2B-A126T mutants at the end of MD simulation (Fig. S7B). The RMSF plot for the UBE2B-A126T mutant also showed decreased RMSF values indicative of reduced flexibility for residues in the backside loop-3 (amino acids 42–51),  $\beta$ -sheet-3, and helix-4 when compared to native UBE2B (Fig. 5A). Moreover, *hbond* analysis showed that the A126T mutation increased the number of hydrogen bonds at the end of simulations of both UBE2A and UBE2B relative to the native protein (Fig. S7C), implying that the threonine substitution decreases overall flexibility or causes compaction of the structures of UBE2A and UBE2B.

MD simulations for the A126F mutation in UBE2A or UBE2B showed the following: The RMSD plot for the UBE2B-A126F mutant showed significant deviation from that of native UBE2B (Fig. S7A, top right panel), suggesting that the bulky phenylalanine substitution in helix-3 adversely impacts the backbone C $\alpha$  atoms to drastically alter the global structure of UBE2B. High RMSF values indicating increased flexibility were evident for residues adjacent to the introduced mutation in helix-3 including the gateway S120 residue in both UBE2A-A126F and UBE2B-A126F mutants when compared to their native proteins (Fig. 5A). Moreover, considerable increases in flexibility were also evident in distant-site residues of the backside region in loop-3 and  $\beta$ -sheet-3 in the UBE2B-A126F mutant (Fig. 5A). Matching well with the destabilization of local and/or global protein structure, *hbond* analysis revealed that the A126F substitution decreased the number of hydrogen bonds in UBE2B at the end of the MD simulation (Fig. S7C, right panel). The DSSP plots further accentuated the destabilizing effect of the A126F mutation, as multiple secondary structures in both UBE2A and UBE2B were either disrupted or reorganized during the course of the simulation (Fig. S6B). These computational simulation studies suggested that like

their disruptive effects on yeast Rad6, mutations in A126 of helix-3 also adversely affected the structures of human UBE2A and UBE2B, with UBE2B appearing to be more sensitive to structural perturbations from the A126 mutations.

#### A126 mutation perturbs the catalytic pocket residues of human Rad6b/UBE2B

Next, we used NMR to experimentally test the effects of A126 mutation on the structure of a human Rad6 homolog. We focused on the UBE2B-A126F mutation, as our computer simulations indicated that it is a severe destabilizing mutation (Figs. 5A and S7; Table S1). We expressed and purified from bacteria  $^{15}\text{N}$  isotope-labeled WT UBE2B or the mutant UBE2B-A126F and recorded their two-dimensional  $^{15}\text{N}$ - $^1\text{H}$  HSQC NMR spectra. We performed residue assignments on the NMR spectra obtained for WT UBE2B using a published dataset (63). The NMR spectrum for the UBE2B-A126F mutant was then superimposed on the assigned NMR spectra for WT UBE2B. There was no overlap of NMR signals obtained for many residues in the UBE2B-A126F mutant with the WT UBE2B (Fig. 5B), indicating that the mutation causes severe structural perturbations within the protein. Quantitation of chemical shift perturbations in the UBE2B-A126F mutant relative to native UBE2B and their subsequent placement on the crystal structure showed that perturbations occurred at multiple residues throughout the mutant protein both close to the site of introduced mutation in  $\alpha$ -helix-3 and at distant sites including at the N-terminus (Fig. 5C). Importantly, drastic perturbations were observed for residues H78, N80, C88, and S120 that form the catalytic pocket of UBE2B (Fig. 5C).

#### A126 mutation adversely affects the solubility and activity of human Rad6b/UBE2B

When heterologous proteins overexpressed in bacteria fail to attain a soluble or native conformation and remain unfolded, they form insoluble protein aggregates termed inclusion bodies (82). WT UBE2B was highly soluble when overexpressed in bacteria, (Fig. 6A, see lanes 4–5), indicating that it is a well-folded protein. In stark contrast, a large amount of the overexpressed UBE2B-A126F mutant was detected in insoluble pellet fraction (Fig. 6A, see lanes 9–10), suggesting that the protein was misfolded or unfolded. This result is consistent with the computational predictions and results from NMR experiments (Figs. 5, B and C and S7, Table S1) and further demonstrates that the A126F mutation in helix-3 destabilizes or disorganizes the protein structure.

Given the disruptions to the catalytic pocket in the UBE2B-A126F mutant (Fig. 5), we performed *in vitro* ubiquitination assays to test the effects of these structural changes on the enzyme activity. Recombinant WT UBE2B or the UBE2B-A126F mutant were expressed and purified from bacteria

structure Rad6 (PDB: 1AYZ) using UCSF Chimera. CSPs were quantified for each mutant from the overlay of their NMR spectrum with that of WT Rad6 (panel B). No overlap of the NMR signal in the mutant relative to the WT was scored as 1, and partial overlap was scored as 0.5. Key residues of the catalytic pocket (green dotted circle) and the site of each A126 mutation in helix-3 are indicated. C, C-terminus; HSQC, heteronuclear single quantum coherence; N, N-terminus; Rad6, Radiation sensitive 6; RMSF, root-mean-square fluctuation.

## Alanine-126 mutations in Rad6-family E2 enzymes

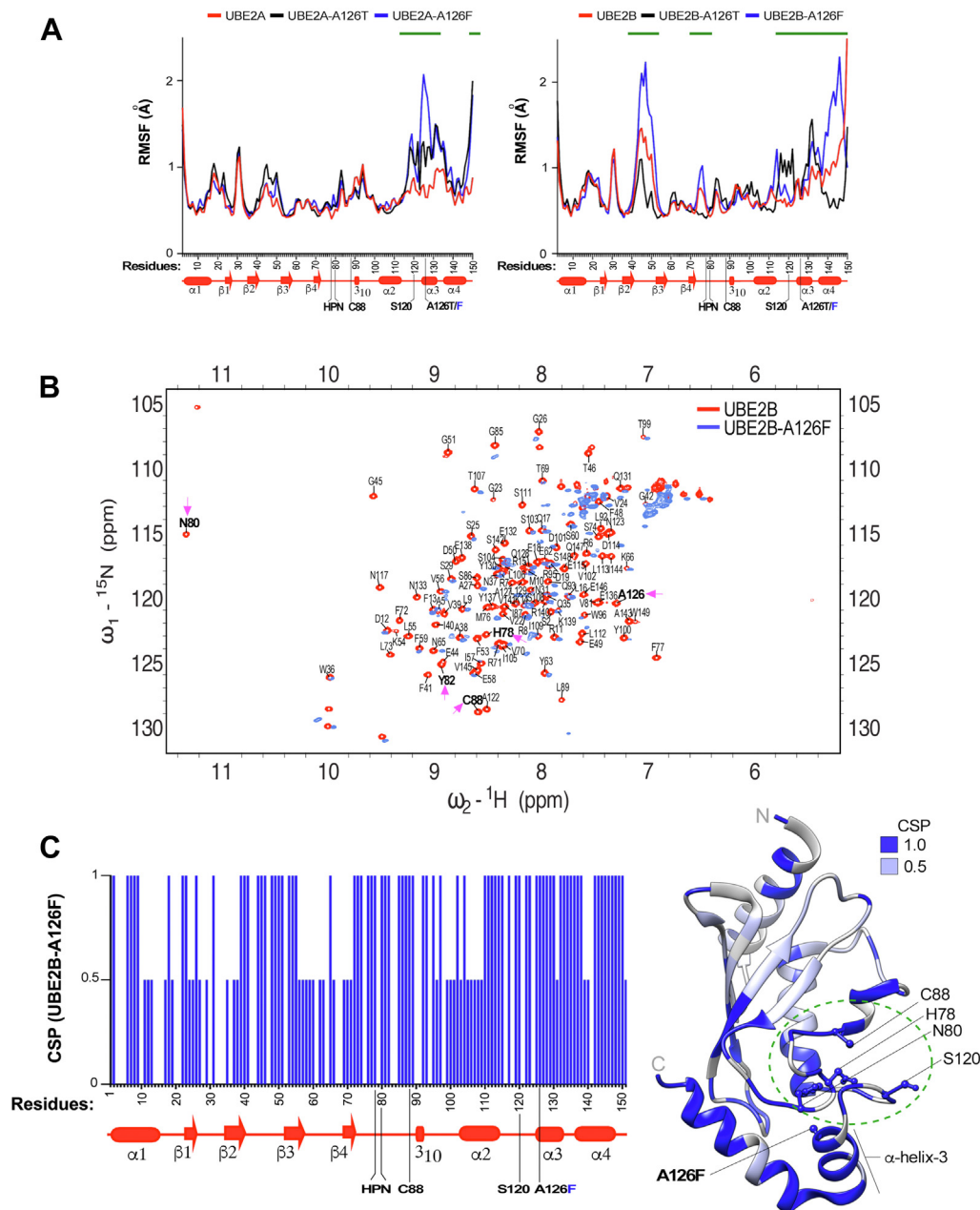


**Figure 5. A126 mutations disorganize the structures of UBE2A and UBE2B.** *A*, RMSF analyses of WT UBE2A or UBE2B (red) and proteins with mutations A126T (black) and A126F (blue). Green lines indicate residues with increased or decreased RMSF values in the mutants relative to WT UBE2A or UBE2B. Schematics below the plots show the secondary structures of the proteins. *B*, overlay of the  $^1\text{H}$ - $^{15}\text{N}$  HSQC spectrum for UBE2B-A126F (blue) on that obtained for WT UBE2B (red). Magenta arrows point to a complete absence of NMR signal or a drastic chemical shift perturbation for the indicated residues of the catalytic pocket in the mutant compared to WT. *C*, left, histogram of the chemical shift perturbation (CSP) at each residue in the mutant. Schematic below the histogram shows the positions of various secondary structures. Right, CSPs, scored as described in (C), mapped onto the crystal structure of UBE2B (PDB: 2YB6) using UCSF Chimera. Key residues of the catalytic pocket of UBE2B (green dotted circle) and the site of A126F mutation in helix-3 are indicated. C, C-terminus; HSQC, heteronuclear single quantum coherence; N, N-terminus; RMSF, root-mean-square fluctuation.

and then used in *in vitro* ubiquitination assays using histone H2B as the substrate. WT UBE2B efficiently mono-ubiquitinated or polyubiquitinated the substrate histone H2B, whereas no mono-ubiquitinated or polyubiquitinated H2B was observed in the presence of the UBE2B-A126F mutant (Fig. 6B). UBE2A and UBE2B show robust *in vitro* ubiquitin chain formation activity in the absence of an E3 ligase or a substrate protein (63) (Fig. S2). This intrinsic *in vitro* ubiquitin chain formation activity of UBE2B was severely compromised

by the A126F mutation (Fig. 6C). Collectively, our findings from MD simulations, NMR, and functional assays suggest that mutation in A126 residue in helix-3 disrupts the enzymatic activity of the human Rad6 homolog as well.

### A126 mutations inhibit ubiquitin charging and discharging of yeast Rad6 and human UBE2B

During the ubiquitination cascade, the E1 ubiquitin-activating enzyme transfers ubiquitin onto the active site

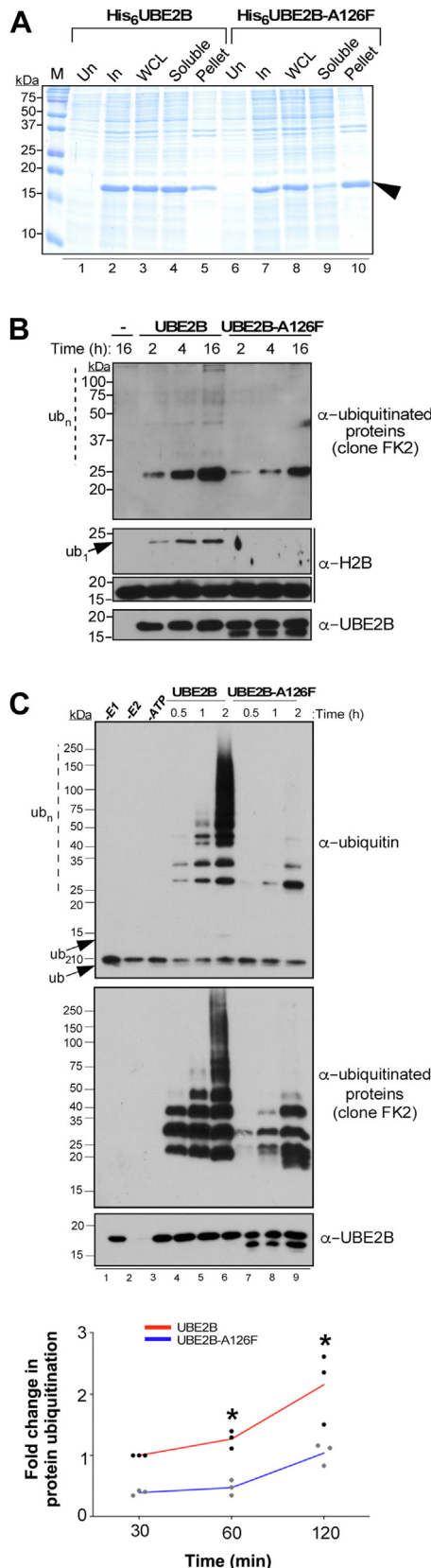


**Figure 6. A126 mutation adversely affects solubility and activity of UBE2B.** A, assessment of solubility of His<sub>6</sub>-tagged UBE2B or UBE2B-A126F (arrowhead) by SDS-PAGE of uninduced (Un) and induced (In) bacterial cells, whole-cell lysate (WCL), and soluble and pellet (or insoluble) fractions. B, *in vitro* ubiquitination assay using recombinant WT UBE2B or the UBE2B-A126F mutant was performed essentially as described for Figure 3A; except,

cysteine of an E2 enzyme *via* a thioester bond and thus an E2 into a catalytically active state. Structure-function studies of E2s in complex with the Uba1 E1 enzyme have shown that residues of helix-3 are part of the E1-E2 interaction interface (83–85). Thus, one could envisage that mutations in A126 could impede the initial ubiquitin charging step to adversely affect the enzymatic activities of yeast or human Rad6. To test this possibility, we assayed the ubiquitin charging of WT or A126 mutant Rad6 by the Uba1 E1 enzyme *in vitro*. To prevent ubiquitin chain formation by E2 enzyme (Fig. S2), a mutant ubiquitin lacking all its lysine residues was used in this charging reaction. Both rad6-A126T and rad6-A126F mutants showed a significant ~2-fold reduction in their ubiquitin-charged or enzymatically active form when compared to the control WT Rad6 (Fig. 7A). Like its yeast counterpart, the UBE2B-A126F mutant also showed a decrease in its ubiquitin-charged form when compared to control UBE2B (Fig. 7B). Thus, these results show that mutation in A126 residue in helix-3 impairs the initial ubiquitin charging step of yeast and human Rad6 proteins.

Superposition of the structures of yeast Rad6 and human UBE2A or UBE2B onto the reported structure of Ubc9 E2 in the act of conjugating SUMO onto substrate RanGAP1(86) (Figs. 8 and S8) showed that helix-3 is present at the E2-substrate interaction interface. Hence, we postulated that A126 mutation in helix-3 might impinge on the discharging step or ubiquitin transfer by Rad6 E2 onto its substrate. To test this possibility, the ubiquitin-charged WT or A126 mutant Rad6 was incubated with substrate histone H2B in *in vitro* ubiquitination reaction. A 2.5 times excess amount of rad6-A126T or rad6-A126F mutant was used in this reaction to account for their reduced ubiquitin charging by the E1 enzyme (Fig. 7A). As shown in Figure 7C, active Rad6 was able to effectively ubiquitinate substrate histone H2B. In contrast, the charged rad6-A126T and rad6-A126F mutants failed to transfer ubiquitin onto histone H2B. We were unable to obtain ubiquitin discharging for human UBE2B or UBE2B-A126F. Nevertheless, our results show that mutation in A126 residue can inhibit Rad6's ability to perform the final ubiquitin transfer onto its substrates. Taken together, our findings from *in vitro* ubiquitination experiments reveal the key roles for helix-3 in the initial ubiquitin charging and the final discharging steps during the catalytic activity of Rad6 family E2 enzymes.

reactions were incubated at 37 °C for the indicated time. Reaction without the E2 enzyme (-) served as a control. C, *in vitro* ubiquitin chain formation assay was performed using recombinant WT UBE2B or the UBE2B-A126F mutant for the indicated time points. Control reactions without human Uba1 (-E1) or UBE2B (-E2) or omitting ATP were also performed. Blots were probed with antibodies recognizing ubiquitin, mono-, or poly-ubiquitinated UBE2B; In panel b, Ub<sub>n</sub>, ubiquitin chains or polyubiquitinated UBE2B; In panel c, Ub, ubiquitin; Ub<sub>1</sub>, monoubiquitinated H2B; Ub<sub>2</sub>, diubiquitin; Ub<sub>n</sub>, polyubiquitinated H2B.

## Alanine-126 mutations in Rad6-family E2 enzymes

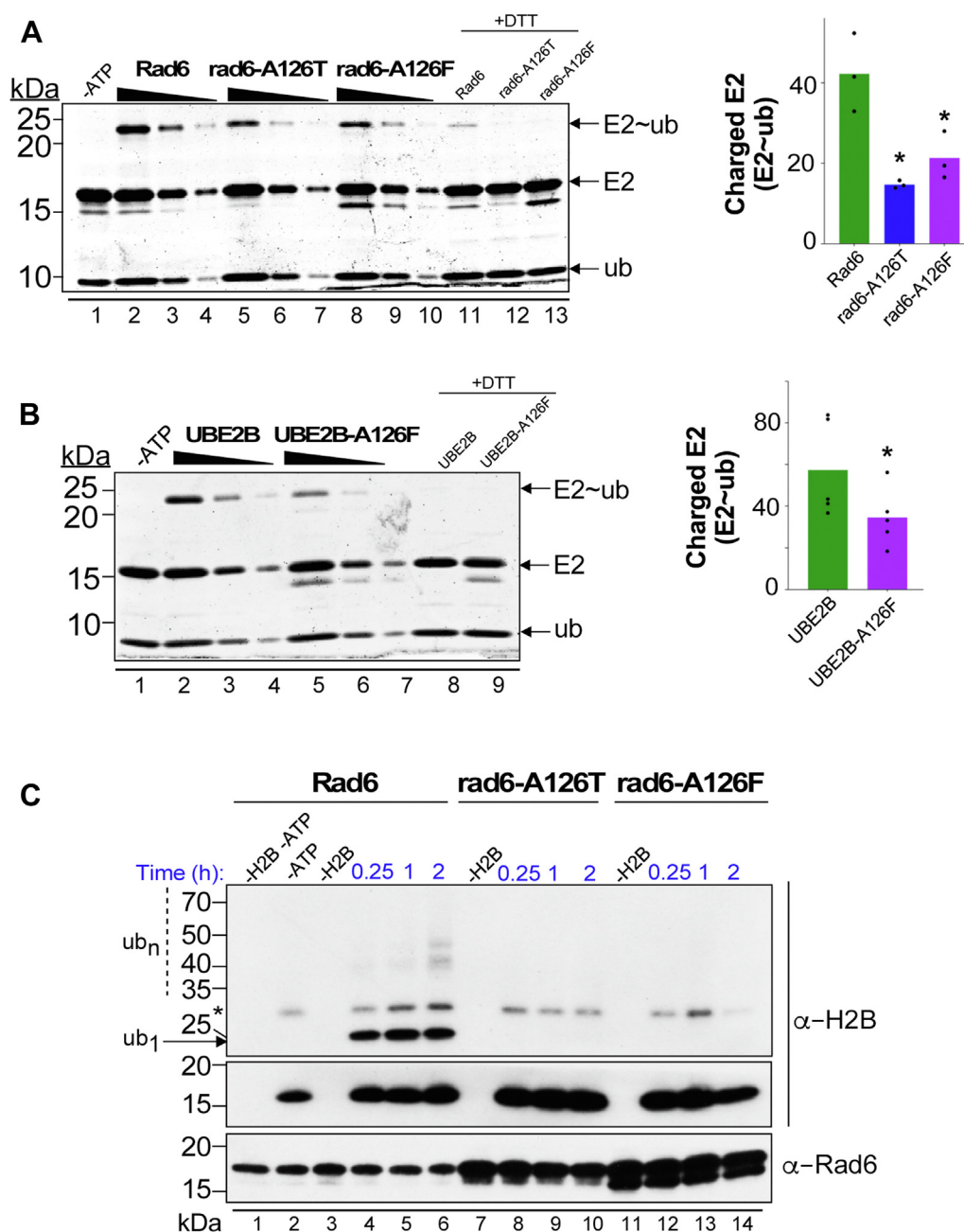


**Figure 7. A126 mutations inhibit the charging and/or discharging abilities of yeast and human Rad6 proteins.** A, WT or A126 mutant Rad6 (50  $\mu$ M) were charged with ubiquitin no-lysine (K0) mutant in an *in vitro* reaction containing Uba1 E1 by incubating at 30 °C for 5 min. Reactions were quenched with nonreducing dye to retain the E2 charged with ubiquitin *via* the labile thioester linkage (E2~ub). Control reactions with a reducing agent treatment (+DTT) or without ATP were also performed. Plot shows the amount of ubiquitin charged WT or mutant Rad6 quantified by densitometry of SYPRO Ruby-stained SDS-PAGE gels from three independent reactions. B, UBE2B or UBE2B-A126F mutant were charged and quantified as described for panel (A), except incubation was done at 32 °C for 5 min. Asterisk, statistical significance was calculated using Student's *t* test, *p*-value < 0.05, from five independent reactions. C, after charging reactions were quenched with EDTA, WT Rad6 (50  $\mu$ M) or 2.5 times excess rad6-A126T or rad6-A126 mutant were incubated with substrate histone H2B (0.2  $\mu$ M) at 30 °C for the indicated time points. The reactions were resolved by SDS-PAGE prior to immunoblotting with anti-H2B or anti-Rad6 antibody. The asterisk indicates a cross-reacting protein. Reactions without H2B and/or ATP (-) served as controls. Rad6, Radiation sensitive 6; Ub<sub>1</sub>, monoubiquitinated H2B; Ub<sub>n</sub>, multi-ubiquitinated H2B.

### Discussion

Rad6, a multifunctional protein in yeast, regulates telomeric gene silencing *via* histone H2BK123 monoubiquitination, protein homeostasis by polyubiquitination of N-degron substrates, and DNA repair *via* monoubiquitination of PCNA and polyubiquitination of Sml1 (28–32, 34–36, 38–42). Here, we demonstrated that threonine or phenylalanine substitution at

A126 in the  $\alpha$ -helix-3 of Rad6 compromises its ability to monoubiquitinate and polyubiquitinate these target proteins. We also showed that interactions of Rad6 with its various partner E3 ligases, which are necessary for *in vivo* ubiquitination of these target proteins, are not disrupted by mutations at A126. Instead, A126 mutations deform the structure of Rad6 and perturb key residues of the catalytic pocket to

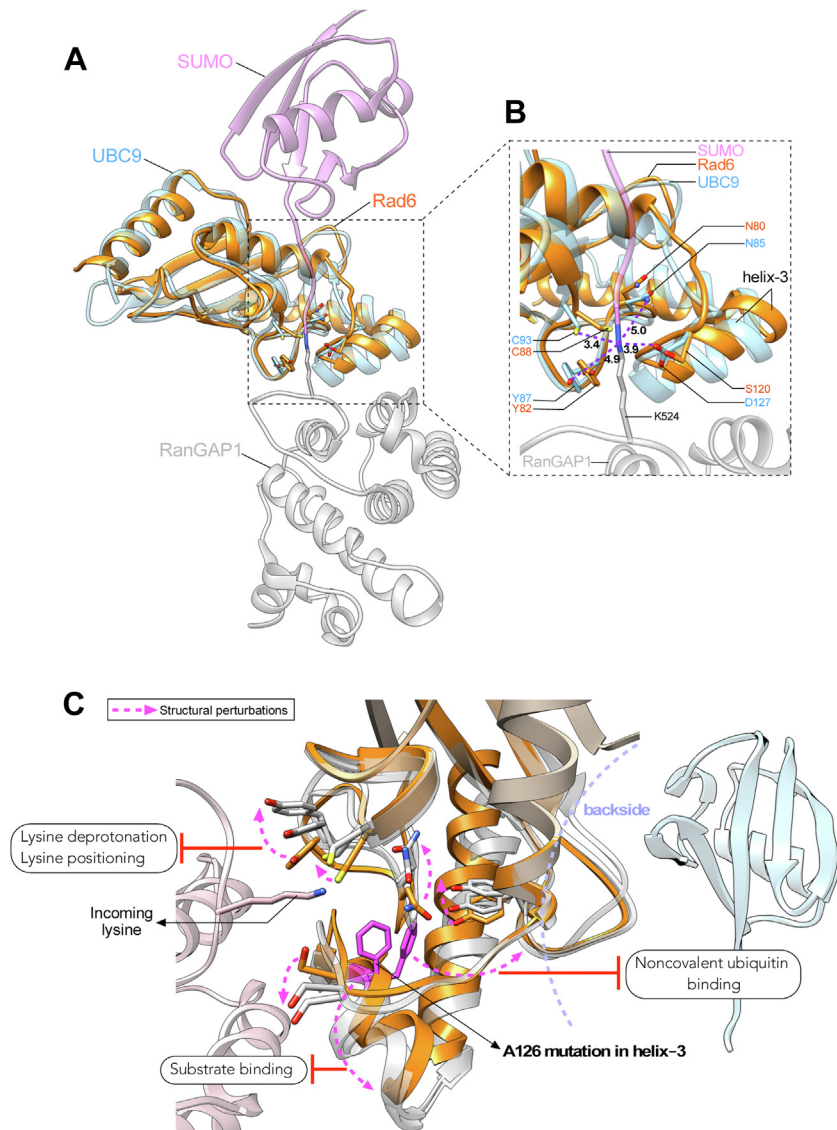


**Figure 8. Models for the contributions of helix-3 to the structure and functions of E2 enzymes.** *A*, structure of Rad6 (PDB ID: 1AYZ) was superposed onto that of UBC9 E2 enzyme in the cocrystal structure of UBC9-SUMO-RanGAP1 (PDB ID: 1Z55) to show the proximity of helix-3 of Rad6 to its catalytic pocket, ubiquitin, and the incoming lysine of a substrate protein. *B*, zoomed image shows the location and distances of the key residues of the catalytic pocket from the isopeptide bond. Also, shown are the distances in angstroms (Å) of the residues of the catalytic pocket in UBC9 to the isopeptide bond between SUMO and target K524 in substrate RanGAP1. *C*, a generalized model to explain how mutation in helix-3 causes local and long-distance structural perturbations (dotted arrows) at catalytically key residues and secondary structures of Rad6 or its homologs UBE2A or UBE2B, and perhaps E2 enzymes in general, to inhibit their catalysis-related transactions with ubiquitin or ubiquitin-like modification and substrate proteins.

inhibit the intrinsic enzymatic activity and to decrease overall protein stability. Thus, our structure-function studies uncover the molecular underpinnings for the phenotypes displayed by yeast with the *rad6-A126T* allele, namely, defects in telomeric silencing, N-end rule degradation, and sensitivity to genotoxic agents, which were first reported over 2 decades ago (53). Moreover, we demonstrated that the bulkier phenylalanine substitution at A126 of helix-3 severely disorganizes local as well as global structures of yeast Rad6 and its human homologs, especially UBE2B, and significantly inhibits their activities. Overall, our studies show that mutations in the conserved helix-3 can disrupt both structure and catalytic functions of yeast and human Rad6 E2 ubiquitin-conjugating enzymes.

Structure-function studies have shown that residues of helix-3 are part of the E1-E2 interaction interface and important for the initial E1-mediated ubiquitin charging of an E2 enzyme (83–85). Here, we show that helix-3 not only functions in the initial ubiquitin charging step of Rad6 family enzymes but also in their ability to perform the transfer of ubiquitin onto substrate proteins (Fig. 7). Below, we put forth various scenarios by which helix-3 could participate in the final ubiquitin discharging step of Rad6 and its homologs and E2 enzymes in general. Residues in the catalytic pocket of E2 enzymes are implicated in deprotonating the  $\epsilon$ -amino group of substrate lysine and converting it into a nucleophile, which then attacks the thioester adduct formed between the E2 active-site cysteine and ubiquitin or ubiquitin-like

## Alanine-126 mutations in Rad6-family E2 enzymes

modifications (e.g., SUMO) (87, 88). Two mechanisms proposed to explain how residues in the E2 catalytic pocket perform lysine deprotonation are as follows: (1) they may act as proton acceptors for the incoming substrate lysine, as reported for H94 in UBE2G2 and D117 in UBE2D1 (89, 90) or (2) they may form a microenvironment that reduces the pKa of the incoming lysine, as reported for residues N85, Y87, and D127 of UBC9, the SUMO-specific E2(87). From the crystal structure of UBC9-SUMO-substrate RanGAP1(86) (Fig. 8A), it is evident that the active-site cysteine and the key residues implicated in lysine deprotonation (N85, Y87, and D127) are all in close proximity to the incoming lysine (~3–5 Å). The optimal distance between the E2 cysteine and the acceptor lysine of the substrate proteins for the transfer of Ub/Ubl is expected to be between 2 to 2.5 Å (91). Therefore, even small perturbations to the conformation of the active-site cysteine and/or other residues of the catalytic pocket of E2 enzymes can alter their operational distance from Ub/Ubl or the substrate lysine to disrupt the conjugation activity.

To further address how structural perturbations caused by mutations in helix-3 might impinge on the enzymatic activities of Rad6 and its human homologs, we superposed the structures of yeast Rad6 and human UBE2A or UBE2B onto the reported structure for the Ubc9 E2 in the act of conjugating SUMO onto substrate RanGAP1(86) (Figs. 8B and S8), which showed that the catalytic pocket residues of yeast and human Rad6 E2 proteins are spatially positioned very similar to their counterparts in UBC9. Importantly, these catalytically key residues are present adjacent to or contiguous with helix-3 in Rad6 and its human homologs. Our MD simulations and NMR experiments show that mutations in helix-3 perturb the active-site cysteine and other residues of the catalytic pockets of yeast and human Rad6 proteins (Figs. 4 and 5). We therefore propose that mutations in helix-3 cause structural changes that alter the distances of the key residues of the catalytic pockets of Rad6 and its human homologs from ubiquitin and/or substrate lysine (Fig. 8C). Thus, mutations in the conserved helix-3 can block ubiquitination activity, as demonstrated by our *in vitro* and/or *in vivo* studies, by causing conformational changes to the critical residues involved in catalysis.

In addition to directly altering the position of the active-site cysteine, mutations in helix-3 can also disrupt the ubiquitin-conjugation activity of yeast or human Rad6 enzymes in other ways. In Rad6, UBE2A, UBE2B, and other E2 enzymes, the catalytic pocket is buttressed by loop-8 or the active-site cleft, which serves as the gate into the active-site. Studies of UBE2K and UBC13 have shown that the opening and closing of the active-site gate is precisely balanced and that even small deviations in gating impair the functions of UBC13 during DNA damage (92–94). A conserved serine or aspartate, termed the gateway residue, is present in the active-site cleft of E2 enzymes and regulates ubiquitination (22). S120 is the gateway residue in Rad6 and its human homologs. This amino acid corresponds to D117 of UBE2D1 and D127 of UBC9, which are implicated in deprotonating the incoming substrate lysine (87, 89). Phosphorylation of S120 regulates the activities of both Rad6 and UBE2A (51, 95). Although S120 as such as

cannot act as a proton acceptor, modification of S120 with a negatively charged phosphate can mimic the acidic nature of an aspartate, allowing this residue to act as a proton acceptor or as a pKa reducer for the incoming lysine. Therefore, mutations in helix-3 could sway the gating dynamics to promote either an inactive or a constitutively active conformation or, alternatively, could impact S120 phosphorylation to affect substrate lysine deprotonation during ubiquitination.

Residues N85 and Y87 of UBC9 are also implicated in reducing the pKa of the incoming lysine (87). These residues correspond to residues N80 and Y82, respectively, of Rad6 and its human homologs. N80 is part of the evolutionarily conserved HPN motif of E2 enzymes. The HPN motif of E2 enzymes functions in localizing the target lysine and in stabilizing the oxyanion formed in the reaction intermediate during the nucleophilic attack (19, 21). The asparagine in this motif aids in the formation of the isopeptide bond, histidine is necessary for the structure, and proline promotes the stable transition of these two amino acids (20, 21, 52, 93). Recently, UBE2A-Q93E was reported to be a novel pathogenic mutation associated with mild intellectual disability, and this mutation was proposed to disturb the catalytic microenvironment of UBE2A essential for its substrate lysine deprotonation (81). Q93 of Rad6, UBE2A, and UBE2B correspond to the proton acceptor H94 in UBE2G2 (90). Our NMR analyses showed that H78, N80, Y82, and Q93 are all significantly perturbed in rad6-A126T, rad6-A126F, and UBE2B-A126F (Figs. 4 and 5). Thus, it is conceivable that mutations in helix-3 can adversely affect the optimal spatial locations of these catalytically vital residues and thus inhibit their functions in substrate lysine deprotonation or oxyanion stabilization during ubiquitination by Rad6 or UBE2A/B (Fig. 8C).

The backside regions of E2 enzymes, comprised of residues of the four  $\beta$ -sheets, the intervening loops, and the C-terminal ends of helices 1 and 4, is the site of noncovalent interactions with ubiquitin (15, 23, 24, 96). This weak affinity interaction promotes increased processivity of polyubiquitin chain formation by E2 enzymes (96). Our RMSF analyses and NMR studies revealed that A126 mutations in helix-3 perturb the conformations of the backside regions of yeast Rad6 and its human homolog(s), especially loop-3 and the C-terminal end of helix-4 (Figs. 4 and 5). Therefore, one could further speculate that the weak-affinity interactions of ubiquitin with the backsides of Rad6 and its human homologs may be abolished because of the structural disruptions caused by helix-3 mutations, which in turn inhibits their polyubiquitination activities, as seen in our *in vitro* or *in vivo* experiments (Figs. 1D, 2D, 3A and 6, B and C). The proximity of helix-3 to the catalytic pocket and its surface accessibility suggest that it might also play a role in substrate recognition by E2 enzymes. Indeed, the helix-3 of UBC9 interacts with the substrate Ran-GAP1 (87) (Fig. 8A). Thus, mutations in helix-3 could prevent substrate binding or correct positioning of the incoming lysine (Fig. 8C).

In a simpler analogy, we envision that the conserved helix-3 acts like a lower jaw that controls the movements or functioning of the lips, which correspond to the catalytic pocket of the E2 enzymes. In summary, our studies reveal the important

contributions of the conserved helix-3 to the enzymatic actions of E2 ubiquitin-conjugating enzymes.

## Experimental procedures

### Yeast strains and media

Yeast cells were grown in YPAD broth (1% yeast extract, 2% peptone, 2% dextrose, and 0.004% adenine hemisulfate) or in synthetic dropout (SD) media. Agar (2%) was added to liquid broth to prepare solid media. To create gene KO strains, the coding region of a target gene was replaced in the parental strains (YMH171 (97) and/or DHY214/DHY217) or the W4622-14B (38) strain using PCR products containing ~500 bp each of the promoter and terminator regions of the target gene and the ORF replacement *KanMX6* selection cassette, which were amplified using genomic DNA isolated from the respective deletion mutant strain from the Open Biosystem's yeast deletion collection. Alternatively, a one-step PCR-based gene knockout strategy was performed using pF6a-KanMX or pAG25 (natMX4) or pAG32 (hphMX4) (98) as the template. The *RAD6* coding region was replaced with *URA3* using a construct that contained the *RAD6* promoter and terminator sequences flanking the *URA3* gene, which was linearized with HindIII-BamHI prior to transformation. YMC309 and YMC336 double or triple gene KO strains were created by mating of single or double gene deletion strains, followed by sporulation and tetrad dissection. Genotypes of yeast strains used in this study are listed in Table S2.

### Plasmid constructs

The *RAD6* terminator region (450 bp) was PCR amplified using yeast genomic DNA as the template. The PCR product also contained sequences for a Flag epitope-tag, a stop codon, SpeI, and BamHI sites at the 5'-end and a KpnI site at the 3'-end. This PCR product was digested with SpeI-KpnI and inserted into the same sites in vector pRS314 (*TRP1*, CEN). Into this construct, the *RAD6* promoter region (286 bp), PCR amplified using yeast genomic DNA as template was inserted as a NotI-SpeI-digested fragment, to obtain construct pMC5 (*RAD6 promoter-SpeI-BamHI-Flag-RAD6 terminator, TRP1* CEN). The coding sequence for WT Rad6 without a stop codon was PCR amplified using yeast genomic DNA as the template and additionally contained SpeI and BamHI sites at its 5' and 3' ends, respectively. This PCR product and construct pMC5 were digested with SpeI and BamHI prior to their ligation using T4 DNA ligase (Invitrogen). Substitution mutations were introduced into Rad6 using a PCR-based site-directed mutagenesis approach. For galactose-inducible expression, the DNA fragments encoding Flag-tagged Rad6, rad6-A126T, or rad6-A126F and the terminator sequence were excised using SpeI and KpnI and inserted into the same sites in vector pRS316 (*GAL1 URA3*, CEN).

For proteins used in NMR studies, the WT or mutant *RAD6*-coding region (amino acids 1–150) was PCR amplified from yeast constructs described above and inserted into the NdeI and BamHI sites downstream of sequence encoding the His<sub>6</sub> tag and the thrombin cleavage sequence in bacterial

expression vector pET28a (Novagen). IDT g-blocks fragments were synthesized for WT UBE2A or UBE2B or their mutants and inserted into NdeI-BamHI-digested pET28a by sequence and ligation independent cloning (SLIC) (99). For coexpression of Rad6 (or its mutants) and Bre1, the coding region (amino acids 1–150) of WT Rad6 or an A126 mutant was PCR amplified and inserted by SLIC into BamHI-NotI sites in bacterial expression vector pRSF-Duet (Novagen). Subsequently, the sequence encoding the Bre1 Rad6-binding region (R6BR) (amino acids 1–214) was PCR amplified and inserted between BglII-XhoI sites using SLIC. For coexpression of Rad6 (or its mutants) and Rad18, the sequence encoding the Rad18 Rad6-binding region (R6BR) (amino acids 301–487) and that of the coding region of glutathione-S-transferase (GST) were PCR amplified and then inserted into NdeI-XhoI-digested pRSF-Duet constructs containing WT Rad6 or an A126 mutant sequences using SLIC. The GST protein tag ensured solubility of Rad18R6BR when expressed in *Escherichia coli*.

### Spotting assays

Telomeric silencing reporter strain YZS377 was transformed with either vector pRS314 (*TRP1*, CEN) (100) alone or construct pMC5 or derivatives containing either WT *RAD6* or a mutant (A126T or A126F). These strains were grown overnight at 30 °C with constant shaking in liquid SD media lacking tryptophan (-TRP). Cells (1 A<sub>600</sub> or 1 × 10<sup>7</sup>) were harvested, and a 10-fold serial dilution was performed prior to spotting them onto solid -TRP media. For the silencing assay, the media additionally contained 5-FOA and cells were grown at 30 °C for 2 to 3 days. For UV and other drug sensitivity assays, strain YZS375 was transformed with a plasmid construct to express either WT Rad6 or one of the mutants (rad6-A126T or rad6-A126F). For the UV sensitivity assay, cells were grown and serially diluted as described above and spotted onto solid -TRP plates prior to being exposed to 254 nm UV light for 15 s. The plates were incubated for 2 days at 30 °C prior to imaging. For drug or compound sensitivity assays, serially diluted cells were spotted onto -TRP media 4% bleomycin, 6% ethanol, or 2% formamide. For examining heat sensitivity, cells spotted on -TRP plates were incubated for 2 days at 37 °C.

### β-galactosidase assay

Yeast strain (YZS375) was transformed with either vector pRS314 (*TRP1*, CEN) or construct pMC5 derivative containing either WT *RAD6* or a mutant (*rad6-A126T* or *rad6-A126F*) along with an N-end rule reporter plasmid (pUB23-R-betagal *URA3*, 2μ) (57). These strains were grown in SD media without tryptophan and uracil (SD-TRP-URA) and with raffinose as the sugar source. Reporter expression was induced by the addition of 2% galactose. The LacZ assay was performed using the Yeast β-Galactosidase Assay Kit (Thermo Scientific) and by following the manufacturer's microfuge tube protocol. Three technical and biological replicates were performed for each strain.

## Alanine-126 mutations in Rad6-family E2 enzymes

### Protein expression

The pET-28a-based constructs for the expression of His<sub>6</sub>-tagged WT or mutant Rad6 or UBE2B were transformed into *E. coli* strain BL21-CodonPlus(DE3)-RIL (Agilent Technologies). For expression and purification of the human E1 enzyme, pET3a-hUBA1 (Addgene#63571, kindly provided by Dr Titia Sixma) (101) was transformed into *E. coli* strain BL21-CodonPlus(DE3)-RIL. Overnight cultures were used to seed fresh 1 l of LB medium containing 50 µg/ml kanamycin and 10 µg/ml chloramphenicol at A<sub>600</sub> 0.1 and then grown with shaking at 37 °C to an A<sub>600</sub> 0.6. Protein expression was induced by adding 0.5 mM IPTG (GoldBio) and grown overnight at 16 °C. Cells were harvested by centrifugation at 6000 rpm for 15 min at 4 °C. The expression plasmid for yeast H2B in pET11a was transformed into *E. coli* BL21-CodonPlus(DE3)-RIL strain and overnight cultures were used to seed 1 l of LB medium containing 100 µg/ml ampicillin and 10 µg/ml chloramphenicol at A<sub>600</sub> 0.1 and then grown with shaking at 37 °C to A<sub>600</sub> 0.6. Protein expression was induced by adding 1 mM IPTG (GoldBio) and grown at 37 °C for 5 h with agitation.

All isotopically labeled proteins were produced in *E. coli* BL21-CodonPlus (DE3)-RIL (Agilent Technologies). To generate the isotopically labeled Rad6, expression was carried out in M9 minimal media supplemented with 3 g/l (<sup>13</sup>C<sub>6</sub>, 99%)-D-glucose and/or 1 g/l (<sup>15</sup>N, 99%)-NH<sub>4</sub>Cl (Cambridge Isotope Laboratories). To generate isotopically labeled rad6-A126T, rad6-A126F, UBE2B, or UBE2B-A126F, the M9 minimal media was supplemented with 1 g/l (<sup>15</sup>N, 99%)-NH<sub>4</sub>Cl and 10 g/l D-glucose. Bacterial cultures were grown in M9 minimal media containing 50 µg/ml kanamycin and 10 µg/ml chloramphenicol at 37 °C to A<sub>600</sub> ~0.6. Heterologous protein expression was induced with 0.5 mM IPTG (GoldBio), and cultures were grown overnight at 19 °C with gentle agitation.

### Metal affinity copurification

The pRSF duet-based constructs to coexpress either WT or mutant Rad6 and Bre1R6BR or Rad18R6BR described above were transformed into *E. coli* BL21-CodonPlus(DE3)-RIL strain. Primary cultures (10 ml) were grown overnight at 37 °C in LB medium containing 30 µg/ml kanamycin and 10 µg/ml chloramphenicol. The overnight culture was then used to seed a fresh 10 ml of LB medium with the indicated antibiotics at A<sub>600</sub> 0.1 and grown with shaking at 37 °C to A<sub>600</sub> 0.6. Protein expression was induced by adding 0.5 mM IPTG (GoldBio) followed by growth overnight at 16 °C. Cells were harvested by centrifugation and resuspended in 1 ml of lysis buffer (25 mM Tris.Cl pH 7.9, 150 mM NaCl, 20 mM imidazole, 0.1% Triton X-100, and 0.1 mM PMSE). The cells were lysed by sonication for 2 min using a Misonix Sonifier and the lysate was clarified by centrifugation at 12,000 rpm for 15 min at 4 °C. Aliquots of cells or lysates were set aside, pre- or post-IPTG addition or clarification by centrifugation, to serve as uninduced or induced and whole cell lysates or soluble fractions.

His<sub>6</sub>-tagged proteins in the clarified supernatant (1 ml) were allowed to bind preequilibrated TALON SuperFlow resin

(Cytiva) with end-over-end mixing for 2 h at 4 °C. Beads were collected by centrifugation at 2800 rpm for 3 min and then washed three times with lysis buffer. The beads were boiled in 2× Laemmli Sample Buffer (Bio-rad). His<sub>6</sub>-tagged WT or mutant Rad6 and copurifying Bre1R6BR or Rad18R6BR in the eluates were separated by 12% SDS-PAGE and visualized by staining with SimplyBlue Safe Stain (Invitrogen). Two independent pull-down or copurification experiments were performed. Stained gels were destained extensively in water, and protein bands were quantified using densitometry (ImageJ).

### Protein purification

Whole cell lysates were prepared in Lysis Buffer (25 mM Tris.Cl pH 7.9, 150 mM NaCl, 20 mM imidazole, 1 mM TCEP, and 1 mM PMSE) and were digested with lysozyme (Sigma) for 20 min on ice and then sonicated using a Misonix Sonifier. The soluble fraction was then obtained by high-speed centrifugation (40,000 rpm, 30 min at 4 °C) using Ti45 rotor in a Beckman OptimaL90-K Ultracentrifuge. Protein purification from the soluble lysate was performed using a three-step chromatography in an ÄKTA FPLC system (Cytiva). The soluble supernatant was first loaded onto a nickel affinity column (HisTrap FF, Cytiva), washed extensively with Lysis Buffer (10 column volumes), and eluted with a 20 to 500 mM imidazole gradient. Fractions with purified protein were combined, and thrombin (10 units; Sigma) was added to remove the His<sub>6</sub> tag, except for proteins in *in vitro* ubiquitin chain formation assay. Samples were dialyzed overnight at 4 °C into a buffer containing 25 mM Tris.Cl pH 7.9, 50 mM KCl, 10% glycerol, 1 mM EDTA, and 1 mM DTT. The dialysate was centrifuged (40,000 rpm, 30 min at 4 °C) and then loaded onto Mono Q anion exchange column (Cytiva) and eluted using a 50 to 1000 mM KCl gradient. Fractions with purified protein were then loaded onto a Superdex 75 gel filtration column (Cytiva) in a buffer containing 25 mM Tris.Cl pH 7.9, 150 mM NaCl, 10% glycerol, 1 mM EDTA, and 1 mM TCEP. For NMR, size-exclusion chromatography was performed in a buffer containing 25 mM sodium phosphate buffer pH 7.5 and 0.5 mM TCEP. Eluted fractions in all chromatography steps were analyzed by SDS-PAGE. The final purified proteins were concentrated using a Vivaspin 10 kDa MWCO Centrifugal Concentrator. For NMR, isotopically labeled and purified UBE2B or UBE2B-A126F were dialyzed into NMR sample buffer (50 mM sodium phosphate buffer pH 8.0, 300 mM NaCl, 1 mM DTT, 10% D<sub>2</sub>O).

To purify yeast histone H2B, cell pellets after IPTG induction were resuspended in lysis buffer (50 mM Tris.Cl, pH 7.5, 100 mM NaCl, 1 mM EDTA, and 1 mM PMSE). Cells were lysed by sonication and the lysate was clarified by centrifugation at 40,000 RPM for 30 min in a Beckman Ultracentrifuge. The soluble fraction was discarded, and the pellet (or inclusion body) fraction was dissolved in an unfolding buffer (7 M guanidium chloride, 20 mM Tris.Cl pH 7.5, and 10 mM DTT). Following centrifugation, the supernatant was directly dialyzed first against 1 l SAU-200 (7 M urea, 20 mM sodium acetate pH 5.2, 200 mM NaCl, 5 mM β-mercaptoethanol, and 1 mM



EDTA) for ~6 h in a cold room and then overnight against fresh 1 l SAU-200, also in the cold room. The dialysate was subsequently loaded onto an SP Sepharose FF column (Cytiva) and eluted with SAU-600 (7 M urea, 600 mM NaCl, 20 mM sodium acetate pH 5.2, 5 mM  $\beta$ -mercaptoethanol, and 1 mM EDTA). Fractions containing histone H2B were pooled and dialyzed into water. Refolding of histone H2B was done by dialysis against 2 l refolding buffer (2 M NaCl, 10 mM Tris.Cl pH 7.5, 1 mM EDTA, and 5 mM  $\beta$ -mercaptoethanol) overnight at 4 °C. Protein in the dialysate was concentrated and purified over a Superdex 75 column in the refolding buffer. Fractions were analyzed on 12% SDS PAGE, and those containing histone H2B were pooled and concentrated using a 10-kDa MWCO Centrifugal Concentrator. For the *in vitro* ubiquitination assay, the purified histone H2B was diluted into a buffer containing 25 mM Tris.Cl pH 7.5, 100 mM NaCl, 1 mM EDTA, and 1 mM DTT.

### Solubility assay

Overnight cultures for *E. coli* cells expressing recombinant UBE2B or UBE2B-A126F were used to seed 10 ml of LB medium containing 50  $\mu$ g/ml kanamycin and 10  $\mu$ g/ml chloramphenicol at  $A_{600}$  0.1 and grown further at 37 °C to  $A_{600}$  0.6, then induced with 0.5 mM IPTG and grown overnight at 19 °C. Cells were harvested and resuspended in a lysis buffer containing 25 mM Tris.Cl pH 7.9, 1 M NaCl, 0.1 mM EDTA, 5 mM imidazole, 1 mM TCEP, and 1 mM PMSF. After sonication, the lysate was centrifuged at 10,000 rpm for 15 min at 4 °C. Aliquots of the lysate before and after centrifugation were designated as whole-cell lysate and soluble lysate fractions, respectively. The pellet or insoluble fraction obtained after centrifugation was dissolved in 0.5 ml lysis buffer. The samples were then resolved by 15% SDS-PAGE and proteins were visualized by staining using SimplyBlue Safe Stain (Invitrogen).

### In vitro ubiquitination assay

The ubiquitination reaction contained 1 $\times$  reaction buffer and 5 mM Mg-ATP (Ubiquitylation Assay Kit; Abcam), 0.1  $\mu$ M recombinant yeast or human GST-Uba1/UBE1 (E1, R&D Systems), 2.5  $\mu$ M recombinant yeast or human ubiquitin (R&D Systems), 0.1  $\mu$ M WT or mutant Rad6 or UBE2B (E2), and 2  $\mu$ M substrate recombinant yeast histone H2B. For yeast Rad6 or its mutant derivatives, the reaction was performed at 30 °C for 15 min, 2 h, or 10 h. For UBE2B or UBE2B-A126F, the reaction was performed at 37 °C for 2 h, 4 h, or 16 h. The reactions were stopped by adding 2 $\times$  Laemmli sample buffer (Bio-Rad) and resolved in a 12% SDS-PAGE prior to immunoblotting with anti-monoubiquitinated and polyubiquitinated protein antibody (clone FK2), anti-yeast H2B antibody, or anti-Rad6 or UBE2B antibody (see details below).

Ubiquitin chain formation assays were performed essentially as described (63): purified Rad6, UBE2A, UBE2B or their mutants (3  $\mu$ M) along with 12  $\mu$ M yeast or human ubiquitin, and 90 nM yeast or human E1 enzyme were included in a buffer (50 mM Tris.Cl pH 8.0, 50 mM NaCl, 50 mM KCl, 10 mM MgCl<sub>2</sub>, 0.1 M DTT, 3 mM ATP) and incubated at

30 °C (for yeast proteins) or 31 °C (for human proteins) at various time points as indicated in the figures. Control reactions lacking either E1 or E2 enzyme or ATP were also performed. The reactions were denatured in SDS-PAGE sample buffer and resolved in Novex 4 to 20% Tris-Glycine gels (Invitrogen) before immunoblotting with anti-ubiquitin or anti-ubiquitinated protein (clone FK2) antibodies or anti-Rad6 or anti-UBE2A or anti-UBE2B antibody (see below). *In vitro* substrate ubiquitination and ubiquitin chain formation assays were confirmed using two independent protein preparations. At least two independent assays were performed and quantitation of immunoblots for anti-ubiquitinated proteins (clone FK2) antibody was performed by densitometry using ImageJ software (<https://imagej.nih.gov/ij/index.html>).

### Coimmunoprecipitation

Log-phase cultures of yeast cells ( $50 \times 10^7$ ) expressing Flag epitope-tagged Rad6 or its mutants were harvested, washed once with PBS, and stored at -80 °C. Cells were lysed by bead beating after resuspension in IP-Lysis Buffer (10 mM Tris.Cl pH 8.0, 100 mM NaCl, 10% glycerol, 0.1% NP-40, and Roche cOmplete EDTA-free protease inhibitor cocktail). The samples were cooled on ice for 5 min between the bead-beat cycles and clarified by two high-speed centrifugations (13,200 rpm at 4 °C) for 20 min and 10 min to obtain the final soluble lysate. Protein estimation was performed using Bio-Rad Protein Assay. An aliquot of the whole cell lysate (50  $\mu$ g) was set aside for 'input'. Lysate (1 mg) from various yeast strains was used in immunoprecipitation with anti-Flag M2 magnetic beads (20  $\mu$ l, Sigma) in a total volume of 1.5 ml of IP-Lysis buffer and incubated with end-over-end rotation for 4 h at 4 °C. The beads were then washed four times with 1 ml IP-Lysis Buffer, and bead-bound proteins were eluted by boiling in 1 $\times$  Laemmli buffer (40  $\mu$ l). Input and eluates were resolved by SDS-PAGE and subjected to Western blotting with a custom anti-Bre1 polyclonal antibody that was raised in rabbit or anti-Flag M2 (Sigma) antibody.

### Protein stability assay

Yeast strains harboring *URA3*, 2 $\mu$  plasmid with *GAL1* promoter-driven *Rad6-2Flag* or *rad6-A126T-2Flag* or *rad6-A126F-2Flag* were grown for 2 days at 30 °C with constant agitation (230 rpm) in SC-URA with raffinose (2%) as the sugar source. After reinoculation and growth in fresh SC-URA with raffinose for 2 to 3 h, expression of Flag-tagged Rad6 or mutants was induced by adding 2% galactose and incubating with agitation for 2 h. Transcription was then shut-off by adding 2% glucose. Cells grown in raffinose or galactose media and at various time points after glucose addition were harvested for extract preparation using the trichloroacetic acid (TCA) lysis method described previously (102). Briefly, log-phase yeast cells ( $20 \times 10^7$ ) were harvested, washed once with PBS and once with 5% TCA (Sigma) before storing at -80 °C. Cell pellets were thawed in 20% TCA, lysed by bead beating and centrifuged (3000 rpm, 5 min at 4 °C). The pellet was resuspended by vortexing in 1 $\times$  Laemmli buffer (62.5 mM Tris.Cl

## Alanine-126 mutations in Rad6-family E2 enzymes

pH 6.8, 10% glycerol, 2% SDS, 0.002% bromophenol blue, 2.5%  $\beta$ -mercaptoethanol). Subsequently, the denatured lysate was neutralized by adding 2 M Tris base before boiling for 8 min in a water bath and then clarified by centrifugation (13,200 rpm, 10 min at 4 °C). Protein concentration of the clarified lysate was measured using DC Protein Assay (Bio-Rad). Protein levels of WT or mutant Rad6 were determined by immunoblotting using anti-Flag M2 antibody (Sigma).

### Immunoblotting

Yeast extracts were prepared using TCA lysis method as described above. Either equal amounts or a serial dilution of the lysates was prepared from various samples before resolving them in SDS-PAGE and transferring onto a polyvinylidene difluoride membrane. Following incubation with primary rabbit or mouse antibody and corresponding HRP-conjugated secondary antibody, protein signals were detected by chemiluminescence using Pierce ECL Plus Western Blotting Substrate (Thermo Scientific) and autoradiography. The following antibodies were used with their source and catalog numbers indicated within parentheses: anti-Flag M2 (F3165; Sigma), anti-Pgk1 (459250; Invitrogen), anti-GFP (AE011, Abclonal), anti-UBE2A (A7744; Abclonal), anti-UBE2B (A6315, Abclonal), anti-V5 (R690, Invitrogen), anti-H2B (39237; Active Motif), anti-H3 (ab1791; Abcam), anti-H3K4me1 (39297; Active Motif), anti-H3K4me2 (399141; Active Motif), anti-H3K4me3 (39159; Active Motif), anti-ubiquitin antibody (ab139467; Abcam); monoubiquitinated and polyubiquitinated conjugates monoclonal antibody (FK2) (HRP conjugate) (BML-PW0150; Enzo Life Sciences), and anti-Rad6 (DZ33919; Boster Bio). Please note that the anti-UBE2B antibody recognizes both UBE2A and UBE2B (Fig. S2).

### Ubiquitin charging and discharging assays

For E2 charging, purified yeast Rad6 or mutants (rad6-A126T or rad6-A126F) (50  $\mu$ M) were added to a ubiquitination reaction containing 50 mM Tris pH 7.4, 50 mM KCl, 50 mM NaCl, 10 mM MgCl<sub>2</sub>, 10 mM ATP, 1  $\mu$ M yeast GST-Uba1 (Bio-technique), and 40  $\mu$ M human ubiquitin no K mutant (Bio-technique), and incubated for 5 min at 30 °C. Purified human UBE2B or UBE2B-A126F mutant (50  $\mu$ M) were charged similarly except incubation was performed at 32 °C. The reactions were quenched in a nonreducing SDS-PAGE sample buffer prior to resolving in 4 to 20% Novex WedgeWell Tris-Glycine gel (Invitrogen). The gel was stained with SYPRO Ruby stain (Invitrogen). Three independent E2-charging reactions were performed, and stained gels were imaged by Typhoon laser-scanner and analyzed by densitometry using ImageJ software.

For discharging experiments, WT or mutant Rad6 was initially charged with ubiquitin as described above and the reaction was quenched with 10 mM EDTA. After charging, WT Rad6 or 2.5 times excess rad6-A126T or rad6-A126F mutant were incubated along with substrate histone H2B (0.2  $\mu$ M) in the ubiquitination buffer described above at 30 °C for 30 min, 1 h, or 2 h. The reactions were quenched with a nonreducing SDS-PAGE sample buffer prior to resolving in 4

to 20% Novex WedgeWell Tris-Glycine gel (Invitrogen) and transferred onto a PVDF membrane for probing with anti-H2B or anti-Rad6 antibody. Three independent discharging reactions were performed. Immunoblots were analyzed by densitometry using ImageJ software.

### Proteasomal inhibition

Yeast episomal plasmids to express Flag epitope-tagged WT Rad6 or mutants rad6-A126T or rad6-A126F were transformed into strain GAC202a (66) and were treated with either DMSO or the proteasome inhibitor MG132 (50  $\mu$ M, Sigma) prior to harvesting and extract preparation by bead beating in SUTE buffer (10 mM Tris.Cl pH 7.5, 8 M Urea, 0.5% SDS, and 10 mM EDTA). Equal amounts of lysates were resolved by SDS-PAGE before immunoblotting with anti-Flag or anti-Pgk1 antibody.

### NMR spectroscopy

NMR data were collected on either a Varian INOVA 500 MHz using a room temperature HCN probe or a Varian INOVA 600 MHz equipped with an HCN Mark2 cryogenic probe. Data were processed and analyzed using NMRpipe (103) and Sparky (104) tools. Complete resonance assignment of WT Rad6 was accomplished using a standard suite of HCN triple resonance experiments (NHcoCA, HNCA, HNCACB, CBCAcoNH, and <sup>15</sup>N-edited NOESY) collected at two temperatures 25 °C and 35 °C with a uniformly labeled <sup>15</sup>N, <sup>13</sup>C, <sup>2</sup>H (~70%) Rad6 sample. Nonuniform sampling routines were used for all 3D HCN experiments (105). Isotope-labeled protein samples for WT or mutant yeast Rad6 or human UBE2B were prepared at 0.75 to 1.0 mM concentration in a buffer containing 25 mM sodium phosphate pH 7.5 and 0.5 mM TCEP. [<sup>15</sup>N, <sup>1</sup>H] HSQC and HSQC-TROSY were recorded for yeast Rad6 and human UBE2B, respectively. Complete assignments for yeast Rad6 are at BMRB with accession code 50964.

Chemical shift perturbations (CSPs) were qualitatively scored as follows: (1) WT and mutant Rad6 or UBE2B were overlaid in Sparky. For each amide signal, an overlap less than one-half the linewidth in either dimension was scored as CSP of 0, an overlap greater than one-half the linewidth and less than a full linewidth was scored as CSP 0.5, and an overlap greater than one linewidth was scored as CSP 1. CSP *versus* residue plots were generated using Graphpad Prism 9.0 (<https://www.graphpad.com/>). CSP values were mapped on the crystal structure of yeast Rad6 (PDB ID: 1AYZ) (67) and human UBE2B (PDB ID: 2YB6) (63) and visualized using UCSF Chimera (106).

### MD simulations

The crystal structures for yeast Rad6 (PDB ID: 1AYZ) (67) and its human homologs UBE2A (PDB ID: 6CYO) (81) and UBE2B (PDB ID: 2YB6) (63) were used to perform the classical MD simulations using the GROMACS 2018.1 package (79). Amber99sb was selected as the forcefield for all the simulations (107). Models for the mutants A126T or A126F were prepared *in silico* using the crystal structures for Rad6, UBE2A,

or UBE2B in YASARA (108). The alanine was replaced with side chains from threonine or phenylalanine followed by a short minimization of 100 ps. A freezing of all residues was performed except for those residues close to the point mutation to avoid any local crashes in the sidechains.

The nine systems (3 native and 6 mutants) prepared above were then solvated explicitly with TIP3P water molecules in a cubic box with a margin of 10 Å as previously described (109) and neutralized by adding sodium counter ions. Energy minimization using the steepest descent method for 5000 steps was carried out to remove any poor van der Waals' contacts in the initial geometry. After the minimization step, two stages of equilibration were conducted: First, NVT (constant number, volume, and temperature) equilibration was performed for 100 ps maintaining a constant temperature of 300 K using V-rescale algorithm (110), with a coupling time of 0.1 ps and separate baths for the solute and the solvent. Second, NPT (constant number, pressure, and temperature) equilibration was then performed with a constant pressure of 1 atm for 100 ps using the Parrinello-Rahman pressure coupling scheme (111), with a time constant of 2 ps. The position-restrained NVT and NPT equilibration steps prompted water relaxation around the protein and reduced the system entropy. The covalent bonds were constrained by using the LINCS (Linear Constraint Solver) algorithm (112), and the electrostatic interactions were computed using the Particle Mesh Ewald method (113), with a cutoff distance of 10 Å. A Lennard-Jones 6-12 potential was used to evaluate van der Waals interactions. Initial velocities were generated randomly using a Maxwell-Boltzmann distribution corresponding to 300 K. Finally, the production run was performed for 100 ns for each prepared system without any restraints at 300 K in the isothermal-isobaric ensemble. A time-step of 0.002 ps was carried out in all the simulations and the MD trajectories were saved every 20 ps.

For trajectory analysis, the structural and conformational changes in the native and the mutant proteins were analyzed by applying *gmx rms* or *gmx rmsf* on trajectories resulting from the production run of simulations. Hydrogen bond interactions were quantified by *gmx hbond* tools of GROMACS program, and DSSP secondary structure evaluations and visualization were performed using VMD software (114) (<http://www.ks.uiuc.edu/Research/vmd/>). The minimized initial structure of each prepared system was used as reference geometry and all output files were analyzed and plots were created using XMGrace tool or Graphpad Prism 9.0. The simulations were repeated three times and the overall trajectories were similar between repetitions.

### Data availability

Complete assignments for yeast Rad6 are at BMRB with accession code 50964.

*Supporting information*—This article contains supporting information (38, 66, 97).

*Acknowledgments*—We are grateful to Drs Alexander Varshavsky, Rodney Rothstein, Brad Cairns, Tim Formosa, Bill Tansey, and the late Joe Horecka for kindly providing us plasmids or yeast strains. We thank Dr Srividya Bhaskara for her valuable suggestions.

*Author contributions*—P. K. S., D. S., A. M. L., J. E. B., S. T., R. G., K. S. R., J. J. S., and M. B. C. investigation; P. K. S. methodology; P. K. S., D. S., J. J. S., and M. B. C. formal analysis; P. K. S. and D. S. software; P. K. S. and D. S. writing—original draft; D. C. S. and M. B. C. funding acquisition; M. B. C. conceptualization; M. B. C. writing—review and editing; M. B. C. supervision; M. B. C. project administration.

*Funding and additional information*—This work was supported by funds provided by the Department of Radiation Oncology, Huntsman Cancer Institute, CCSG Nuclear Control seed grant (P30CA042014) and NIGMS-5R01GM127783-02 to M. B. C.

*Conflict of interest*—The authors declare that they have no known competing financial interests or personal relationships that could have appeared to influence the work reported in this paper.

*Abbreviations*—The abbreviations used are: 5FOA, 5-fluoroorotic acid; CSP, chemical shift perturbation; DSSP, definition of secondary structure of proteins; HSQC, heteronuclear single quantum coherence; Rad6, Radiation sensitive 6; RMSF, root-mean-square fluctuation; SD, synthetic dropout; SLIC, sequence and ligation independent cloning; TCA, trichloroacetic acid.

### References

- Komander, D., and Rape, M. (2012) The ubiquitin code. *Annu. Rev. Biochem.* **81**, 203–229
- Damgaard, R. B. (2021) The ubiquitin system: from cell signalling to disease biology and new therapeutic opportunities. *Cell Death Differ.* **28**, 423–426
- Ciechanover, A. (2015) The unravelling of the ubiquitin system. *Nat. Rev. Mol. Cell Biol.* **16**, 322–324
- Zheng, N., and Shabek, N. (2017) Ubiquitin ligases: structure, function, and regulation. *Annu. Rev. Biochem.* **86**, 129–157
- Hicke, L. (2001) Protein regulation by monoubiquitin. *Nat. Rev. Mol. Cell Biol.* **2**, 195–201
- Sewduth, R. N., Baietti, M. F., and Sablina, A. A. (2020) Cracking the monoubiquitin code of genetic diseases. *Int. J. Mol. Sci.* **21**, 3036
- Sigismund, S., Polo, S., and Di Fiore, P. P. (2004) Signaling through monoubiquitination. *Curr. Top. Microbiol. Immunol.* **286**, 149–185
- Kliza, K., and Husnjak, K. (2020) Resolving the complexity of ubiquitin networks. *Front. Mol. Biosci.* **7**, 21
- Jiang, Y. H., and Beaudet, A. L. (2004) Human disorders of ubiquitination and proteasomal degradation. *Curr. Opin. Pediatr.* **16**, 419–426
- Ciechanover, A., and Schwartz, A. L. (2004) The ubiquitin system: pathogenesis of human diseases and drug targeting. *Biochim. Biophys. Acta* **1695**, 3–17
- Atkin, G., and Paulson, H. (2014) Ubiquitin pathways in neurodegenerative disease. *Front. Mol. Neurosci.* **7**, 63
- Senft, D., Qi, J., and Ronai, Z. A. (2018) Ubiquitin ligases in oncogenic transformation and cancer therapy. *Nat. Rev. Cancer* **18**, 69–88
- Borg, N. A., and Dixit, V. M. (2017) Ubiquitin in cell-cycle regulation and dysregulation in cancer. *Annu. Rev. Cancer Biol.* **1**, 59–77
- Hormaechea-Agulla, D., Kim, Y., Song, M. S., and Song, S. J. (2018) New insights into the role of E2s in the pathogenesis of diseases: lessons learned from UBE2O. *Mol. Cells* **41**, 168–178
- Stewart, M. D., Ritterhoff, T., Klevit, R. E., and Brzovic, P. S. (2016) E2 enzymes: more than just middle men. *Cell Res.* **26**, 423–440
- Ye, Y., and Rape, M. (2009) Building ubiquitin chains: E2 enzymes at work. *Nat. Rev. Mol. Cell Biol.* **10**, 755–764

## Alanine-126 mutations in Rad6-family E2 enzymes

17. Burroughs, A. M., Jaffee, M., Iyer, L. M., and Aravind, L. (2008) Anatomy of the E2 ligase fold: implications for enzymology and evolution of ubiquitin/Ub-like protein conjugation. *J. Struct. Biol.* **162**, 205–218
18. Sung, P., Prakash, S., and Prakash, L. (1990) Mutation of cysteine-88 in the *Saccharomyces cerevisiae* RAD6 protein abolishes its ubiquitin-conjugating activity and its various biological functions. *Proc. Natl. Acad. Sci. U. S. A.* **87**, 2695–2699
19. Sadowski, M., Suryadinata, R., Lai, X., Heierhorst, J., and Sarcevic, B. (2010) Molecular basis for lysine specificity in the yeast ubiquitin-conjugating enzyme Cdc34. *Mol. Cell. Biol.* **30**, 2316–2329
20. Berndsen, C. E., Wiener, R., Yu, I. W., Ringel, A. E., and Wolberger, C. (2013) A conserved asparagine has a structural role in ubiquitin-conjugating enzymes. *Nat. Chem. Biol.* **9**, 154–156
21. Wu, P. Y., Hanlon, M., Eddins, M., Tsui, C., Rogers, R. S., Jensen, J. P., et al. (2003) A conserved catalytic residue in the ubiquitin-conjugating enzyme family. *EMBO J.* **22**, 5241–5250
22. Valimberti, I., Tiberti, M., Lambrugh, M., Sarcevic, B., and Papaleo, E. (2015) E2 superfamily of ubiquitin-conjugating enzymes: constitutively active or activated through phosphorylation in the catalytic cleft. *Sci. Rep.* **5**, 14849
23. Wenzel, D. M., Stoll, K. E., and Kleit, R. E. (2011) E2s: structurally economical and functionally replete. *Biochem. J.* **433**, 31–42
24. Kumar, P., Magala, P., Geiger-Schuller, K. R., Majumdar, A., Tolman, J. R., and Wolberger, C. (2015) Role of a non-canonical surface of Rad6 in ubiquitin conjugating activity. *Nucleic Acids Res.* **43**, 9039–9050
25. Kumar, P., and Wolberger, C. (2015) Structure of the yeast Bre1 RING domain. *Proteins* **83**, 1185–1190
26. Page, R. C., Prunedda, J. N., Amick, J., Kleit, R. E., and Misra, S. (2012) Structural insights into the conformation and oligomerization of E2~ubiquitin conjugates. *Biochemistry* **51**, 4175–4187
27. Sakata, E., Satoh, T., Yamamoto, S., Yamaguchi, Y., Yagi-Utsumi, M., Kurimoto, E., et al. (2010) Crystal structure of UbcH5b~ubiquitin intermediate: insight into the formation of the self-assembled E2~Ub conjugates. *Structure* **18**, 138–147
28. Hoegge, C., Pfander, B., Moldovan, G. L., Pyrowolakis, G., and Jentsch, S. (2002) RAD6-dependent DNA repair is linked to modification of PCNA by ubiquitin and SUMO. *Nature* **419**, 135–141
29. Bailly, V., Lamb, J., Sung, P., Prakash, S., and Prakash, L. (1994) Specific complex formation between yeast RAD6 and RAD18 proteins: a potential mechanism for targeting RAD6 ubiquitin-conjugating activity to DNA damage sites. *Genes Dev.* **8**, 811–820
30. Wood, A., Krogan, N. J., Dover, J., Schneider, J., Heidt, J., Boateng, M. A., et al. (2003) Bre1, an E3 ubiquitin ligase required for recruitment and substrate selection of Rad6 at a promoter. *Mol. Cell* **11**, 267–274
31. Robzyk, K., Recht, J., and Osley, M. A. (2000) Rad6-dependent ubiquitination of histone H2B in yeast. *Science* **287**, 501–504
32. Hwang, W. W., Venkatasubrahmanyam, S., Ianculescu, A. G., Tong, A., Boone, C., and Madhani, H. D. (2003) A conserved RING finger protein required for histone H2B monoubiquitination and cell size control. *Mol. Cell* **11**, 261–266
33. Xiao, T., Kao, C. F., Krogan, N. J., Sun, Z. W., Greenblatt, J. F., Osley, M. A., et al. (2005) Histone H2B ubiquitylation is associated with elongating RNA polymerase II. *Mol. Cell. Biol.* **25**, 637–651
34. Sun, Z. W., and Allis, C. D. (2002) Ubiquitination of histone H2B regulates H3 methylation and gene silencing in yeast. *Nature* **418**, 104–108
35. Briggs, S. D., Xiao, T., Sun, Z. W., Caldwell, J. A., Shabanowitz, J., Hunt, D. F., et al. (2002) Gene silencing: trans-histone regulatory pathway in chromatin. *Nature* **418**, 498
36. Nakanishi, S., Lee, J. S., Gardner, K. E., Gardner, J. M., Takahashi, Y. H., Chandrasekharan, M. B., et al. (2009) Histone H2BK123 monoubiquitination is the critical determinant for H3K4 and H3K79 trimethylation by COMPASS and Dot1. *J. Cell Biol.* **186**, 371–377
37. Chandrasekharan, M. B., Huang, F., Chen, Y. C., and Sun, Z. W. (2010) Histone H2B C-terminal helix mediates trans-histone H3K4 methylation independent of H2B ubiquitination. *Mol. Cell. Biol.* **30**, 3216–3232
38. Andreson, B. L., Gupta, A., Georgieva, B. P., and Rothstein, R. (2010) The ribonucleotide reductase inhibitor, Sml1, is sequentially phosphorylated, ubiquitylated and degraded in response to DNA damage. *Nucleic Acids Res.* **38**, 6490–6501
39. Ju, D., Wang, X., Xu, H., and Xie, Y. (2008) Genome-wide analysis identifies MYND-domain protein Mub1 as an essential factor for Rpn4 ubiquitylation. *Mol. Cell. Biol.* **28**, 1404–1412
40. Akiyoshi, B., Nelson, C. R., Duggan, N., Ceto, S., Ranish, J. A., and Biggins, S. (2013) The Mub1/Ubr2 ubiquitin ligase complex regulates the conserved Dsn1 kinetochore protein. *PLoS Genet.* **9**, e1003216
41. Sung, P., Berleth, E., Pickart, C., Prakash, S., and Prakash, L. (1991) Yeast RAD6 encoded ubiquitin conjugating enzyme mediates protein degradation dependent on the N-end-recognizing E3 enzyme. *EMBO J.* **10**, 2187–2193
42. Dohmen, R. J., Madura, K., Bartel, B., and Varshavsky, A. (1991) The N-end rule is mediated by the UBC2(RAD6) ubiquitin-conjugating enzyme. *Proc. Natl. Acad. Sci. U. S. A.* **88**, 7351–7355
43. Pan, M., Zheng, Q., Wang, T., Liang, L., Mao, J., Zuo, C., et al. (2021) Structural insights into Ubr1-mediated N-degron polyubiquitination. *Nature* **600**, 334–338
44. Watkins, J. F., Sung, P., Prakash, S., and Prakash, L. (1993) The extremely conserved amino terminus of RAD6 ubiquitin-conjugating enzyme is essential for amino-end rule-dependent protein degradation. *Genes Dev.* **7**, 250–261
45. Bailly, V., Prakash, S., and Prakash, L. (1997) Domains required for dimerization of yeast Rad6 ubiquitin-conjugating enzyme and Rad18 DNA binding protein. *Mol. Cell. Biol.* **17**, 4536–4543
46. Kim, J., and Roeder, R. G. (2009) Direct Bre1-Paf1 complex interactions and RING finger-independent Bre1-Rad6 interactions mediate histone H2B ubiquitylation in yeast. *J. Biol. Chem.* **284**, 20582–20592
47. Turco, E., Gallego, L. D., Schneider, M., and Kohler, A. (2015) Mono-ubiquitination of histone H2B is intrinsic to the Bre1 RING domain-Rad6 interaction and augmented by a second Rad6-binding site on Bre1. *J. Biol. Chem.* **290**, 5298–5310
48. Morrison, A., Miller, E. J., and Prakash, L. (1988) Domain structure and functional analysis of the carboxyl-terminal polyacidic sequence of the RAD6 protein of *Saccharomyces cerevisiae*. *Mol. Cell. Biol.* **8**, 1179–1185
49. Sung, P., Prakash, S., and Prakash, L. (1988) The RAD6 protein of *Saccharomyces cerevisiae* polyubiquitinates histones, and its acidic domain mediates this activity. *Genes Dev.* **2**, 1476–1485
50. Raboy, B., and Kulka, R. G. (1994) Role of the C-terminus of *Saccharomyces cerevisiae* ubiquitin-conjugating enzyme (Rad6) in substrate and ubiquitin-protein-ligase (E3-R) interactions. *Eur. J. Biochem.* **221**, 247–251
51. Wood, A., Schneider, J., Dover, J., Johnston, M., and Shilatifard, A. (2005) The Bur1/Bur2 complex is required for histone H2B monoubiquitination by Rad6/Bre1 and histone methylation by COMPASS. *Mol. Cell* **20**, 589–599
52. Cook, B. W., and Shaw, G. S. (2012) Architecture of the catalytic HPN motif is conserved in all E2 conjugating enzymes. *Biochem. J.* **445**, 167–174
53. Freiberg, G., Mesecar, A. D., Huang, H., Hong, J. Y., and Liebman, S. W. (2000) Characterization of novel rad6/ubc2 ubiquitin-conjugating enzyme mutants in yeast. *Curr. Genet.* **37**, 221–233
54. Boeke, J. D., Trueheart, J., Natsoulis, G., and Fink, G. R. (1987) 5-Fluoroorotic acid as a selective agent in yeast molecular genetics. *Methods Enzymol.* **154**, 164–175
55. Povirk, L. F. (1996) DNA damage and mutagenesis by radiomimetic DNA-cleaving agents: bleomycin, neocarzinostatin and other enediynes. *Mutat. Res.* **355**, 71–89
56. Varshavsky, A. (2011) The N-end rule pathway and regulation by proteolysis. *Protein Sci.* **20**, 1298–1345
57. Bachmair, A., Finley, D., and Varshavsky, A. (1986) *In vivo* half-life of a protein is a function of its amino-terminal residue. *Science* **234**, 179–186
58. Santos-Rosa, H., Schneider, R., Bannister, A. J., Sherriff, J., Bernstein, B. E., Emre, N. C., et al. (2002) Active genes are tri-methylated at K4 of histone H3. *Nature* **419**, 407–411
59. Krogan, N. J., Dover, J., Khorrami, S., Greenblatt, J. F., Schneider, J., Johnston, M., et al. (2002) COMPASS, a histone H3 (lysine 4)

- methyltransferase required for telomeric silencing of gene expression. *J. Biol. Chem.* **277**, 10753–10755
60. Daniel, J. A., Torok, M. S., Sun, Z. W., Schieltz, D., Allis, C. D., Yates, J. R., 3rd, *et al.* (2004) Deubiquitination of histone H2B by a yeast acetyltransferase complex regulates transcription. *J. Biol. Chem.* **279**, 1867–1871
  61. Gardner, R. G., Nelson, Z. W., and Gottschling, D. E. (2005) Ubp10/Dot4p regulates the persistence of ubiquitinated histone H2B: distinct roles in telomeric silencing and general chromatin. *Mol. Cell. Biol.* **25**, 6123–6139
  62. Gallego-Sanchez, A., Andres, S., Conde, F., San-Segundo, P. A., and Bueno, A. (2012) Reversal of PCNA ubiquitylation by Ubp10 in *Saccharomyces cerevisiae*. *PLoS Genet.* **8**, e1002826
  63. Hibbert, R. G., Huang, A., Boelens, R., and Sixma, T. K. (2011) E3 ligase Rad18 promotes monoubiquitination rather than ubiquitin chain formation by E2 enzyme Rad6. *Proc. Natl. Acad. Sci. U. S. A.* **108**, 5590–5595
  64. Jentsch, S., McGrath, J. P., and Varshavsky, A. (1987) The yeast DNA repair gene RAD6 encodes a ubiquitin-conjugating enzyme. *Nature* **329**, 131–134
  65. Samant, R. S., and Frydman, J. (2019) Methods for measuring misfolded protein clearance in the budding yeast *Saccharomyces cerevisiae*. *Methods Enzymol.* **619**, 27–45
  66. Collins, G. A., Gomez, T. A., Deshaies, R. J., and Tansey, W. P. (2010) Combined chemical and genetic approach to inhibit proteolysis by the proteasome. *Yeast* **27**, 965–974
  67. Worthylake, D. K., Prakash, S., Prakash, L., and Hill, C. P. (1998) Crystal structure of the *Saccharomyces cerevisiae* ubiquitin-conjugating enzyme Rad6 at 2.6 Å resolution. *J. Biol. Chem.* **273**, 6271–6276
  68. Ptak, C., Gwozd, C., Huzil, J. T., Gwozd, T. J., Garen, G., and Ellison, M. J. (2001) Creation of a pluripotent ubiquitin-conjugating enzyme. *Mol. Cell. Biol.* **21**, 6537–6548
  69. Hampsey, M. (1997) A review of phenotypes in *Saccharomyces cerevisiae*. *Yeast* **13**, 1099–1133
  70. Khan, F. I., Wei, D. Q., Gu, K. R., Hassan, M. I., and Tabrez, S. (2016) Current updates on computer aided protein modeling and designing. *Int. J. Biol. Macromol.* **85**, 48–62
  71. Karplus, M., and McCammon, J. A. (2002) Molecular dynamics simulations of biomolecules. *Nat. Struct. Biol.* **9**, 646–652
  72. Hollingsworth, S. A., and Dror, R. O. (2018) Molecular dynamics simulation for all. *Neuron* **99**, 1129–1143
  73. Sinha, D., Bialevich, V., Shamayeva, K., Guzanova, A., Sisakova, A., Csefalvay, E., *et al.* (2018) A residue of motif III positions the helicase domains of motor subunit HsdR in restriction-modification enzyme EcoR124I. *J. Mol. Model.* **24**, 176
  74. Garcia, A. E. (1992) Large-amplitude nonlinear motions in proteins. *Phys. Rev. Lett.* **68**, 2696–2699
  75. Zhao, Y., Zeng, C., and Massiah, M. A. (2015) Molecular dynamics simulation reveals insights into the mechanism of unfolding by the A130T/V mutations within the MID1 zinc-binding Bbox1 domain. *PLoS One* **10**, e0124377
  76. Maguid, S., Fernandez-Alberti, S., Parisi, G., and Echave, J. (2006) Evolutionary conservation of protein backbone flexibility. *J. Mol. Evol.* **63**, 448–457
  77. Keskin, O., Jernigan, R. L., and Bahar, I. (2000) Proteins with similar architecture exhibit similar large-scale dynamic behavior. *Biophys. J.* **78**, 2093–2106
  78. Kabsch, W., and Sander, C. (1983) Dictionary of protein secondary structure: pattern recognition of hydrogen-bonded and geometrical features. *Biopolymers* **22**, 2577–2637
  79. Mark James, A., Teemu, M., Roland, S., Szilárd, P., Jeremy, C. S., Berk, H., *et al.* (2015) GROMACS: high performance molecular simulations through multi-level parallelism from laptops to supercomputers. *SoftwareX* **1-2**, 19–25
  80. Rodrigues, C. H., Pires, D. E., and Ascher, D. B. (2018) DynaMut: predicting the impact of mutations on protein conformation, flexibility and stability. *Nucleic Acids Res.* **46**, W350–W355
  81. de Oliveira, J. F., do Prado, P. F. V., da Costa, S. S., Sforca, M. L., Canateli, C., Ranzani, A. T., *et al.* (2019) Mechanistic insights revealed by a UBE2A mutation linked to intellectual disability. *Nat. Chem. Biol.* **15**, 62–70
  82. Baneyx, F., and Mujacic, M. (2004) Recombinant protein folding and misfolding in *Escherichia coli*. *Nat. Biotechnol.* **22**, 1399–1408
  83. Olsen, S. K., and Lima, C. D. (2013) Structure of a ubiquitin E1-E2 complex: insights to E1-E2 thioester transfer. *Mol. Cell* **49**, 884–896
  84. Williams, K. M., Qie, S., Atkinson, J. H., Salazar-Arango, S., Alan Diehl, J., and Olsen, S. K. (2019) Structural insights into E1 recognition and the ubiquitin-conjugating activity of the E2 enzyme Cdc34. *Nat. Commun.* **10**, 3296
  85. Lv, Z., Rickman, K. A., Yuan, L., Williams, K., Selvam, S. P., Woosley, A. N., *et al.* (2017) *S. pombe* Uba1-Ubc15 structure reveals a novel regulatory mechanism of ubiquitin E2 activity. *Mol. Cell* **65**, 699–714.e696
  86. Reverter, D., and Lima, C. D. (2005) Insights into E3 ligase activity revealed by a SUMO-RanGAP1-Ubc9-Nup358 complex. *Nature* **435**, 687–692
  87. Yunus, A. A., and Lima, C. D. (2006) Lysine activation and functional analysis of E2-mediated conjugation in the SUMO pathway. *Nat. Struct. Mol. Biol.* **13**, 491–499
  88. Saha, A., Lewis, S., Kleiger, G., Kuhlman, B., and Deshaies, R. J. (2011) Essential role for ubiquitin-ubiquitin-conjugating enzyme interaction in ubiquitin discharge from Cdc34 to substrate. *Mol. Cell* **42**, 75–83
  89. Zhen, Y., Qin, G., Luo, C., Jiang, H., Yu, K., and Chen, G. (2014) Exploring the RING-catalyzed ubiquitin transfer mechanism by MD and QM/MM calculations. *PLoS One* **9**, e101663
  90. Ju, T., Bocik, W., Majumdar, A., and Tolman, J. R. (2010) Solution structure and dynamics of human ubiquitin conjugating enzyme Ube2g2. *Proteins* **78**, 1291–1301
  91. Verdecia, M. A., Joazeiro, C. A., Wells, N. J., Ferrer, J. L., Bowman, M. E., Hunter, T., *et al.* (2003) Conformational flexibility underlies ubiquitin ligation mediated by the WWP1 HECT domain E3 ligase. *Mol. Cell* **11**, 249–259
  92. Rout, M. K., Hodge, C. D., Markin, C. J., Xu, X., Glover, J. N., Xiao, W., *et al.* (2014) Stochastic gate dynamics regulate the catalytic activity of ubiquitination enzymes. *J. Am. Chem. Soc.* **136**, 17446–17458
  93. Markin, C. J., Saltibus, L. F., Kean, M. J., McKay, R. T., Xiao, W., and Spyropoulos, L. (2010) Catalytic proficiency of ubiquitin conjugation enzymes: balancing pK(a) suppression, entropy, and electrostatics. *J. Am. Chem. Soc.* **132**, 17775–17786
  94. Rout, M. K., Lee, B. L., Lin, A., Xiao, W., and Spyropoulos, L. (2018) Active site gate dynamics modulate the catalytic activity of the ubiquitination enzyme E2-25K. *Sci. Rep.* **8**, 7002
  95. Sarcevic, B., Mawson, A., Baker, R. T., and Sutherland, R. L. (2002) Regulation of the ubiquitin-conjugating enzyme hHR6A by CDK-mediated phosphorylation. *EMBO J.* **21**, 2009–2018
  96. Middleton, A. J., Wright, J. D., and Day, C. L. (2017) Regulation of E2s: a role for additional ubiquitin binding sites? *J. Mol. Biol.* **429**, 3430–3440
  97. Zhang, Y., Sun, Z. W., Iratni, R., Erdjument-Bromage, H., Tempst, P., Hampsey, M., *et al.* (1998) SAP30, a novel protein conserved between human and yeast, is a component of a histone deacetylase complex. *Mol. Cell* **1**, 1021–1031
  98. Goldstein, A. L., and McCusker, J. H. (1999) Three new dominant drug resistance cassettes for gene disruption in *Saccharomyces cerevisiae*. *Yeast* **15**, 1541–1553
  99. Li, M. Z., and Elledge, S. J. (2012) Slic: a method for sequence- and ligation-independent cloning. *Methods Mol. Biol.* **852**, 51–59
  100. Sikorski, R. S., and Hieter, P. (1989) A system of shuttle vectors and yeast host strains designed for efficient manipulation of DNA in *Saccharomyces cerevisiae*. *Genetics* **122**, 19–27
  101. Pichler, A., Knipscheer, P., Oberhofer, E., van Dijk, W. J., Korner, R., Olsen, J. V., *et al.* (2005) SUMO modification of the ubiquitin-conjugating enzyme E2-25K. *Nat. Struct. Mol. Biol.* **12**, 264–269
  102. Chandrasekharan, M. B., Huang, F., and Sun, Z. W. (2011) Decoding the trans-histone crosstalk: methods to analyze H2B ubiquitination, H3 methylation and their regulatory factors. *Methods* **54**, 304–314

## Alanine-126 mutations in Rad6-family E2 enzymes

103. Delaglio, F., Grzesiek, S., Vuister, G. W., Zhu, G., Pfeifer, J., and Bax, A. (1995) NMRPipe: a multidimensional spectral processing system based on UNIX pipes. *J. Biomol. NMR* **6**, 277–293
104. Goddard, T. D., and Kneller, D. G. (2008) SPARKY 3. University of California, San Francisco, CA
105. Hyberts, S. G., Arthanari, H., and Wagner, G. (2012) Applications of non-uniform sampling and processing. *Top. Curr. Chem.* **316**, 125–148
106. Pettersen, E. F., Goddard, T. D., Huang, C. C., Couch, G. S., Greenblatt, D. M., Meng, E. C., et al. (2004) UCSF Chimera—a visualization system for exploratory research and analysis. *J. Comput. Chem.* **25**, 1605–1612
107. Hornak, V., Abel, R., Okur, A., Strockbine, B., Roitberg, A., and Simmerling, C. (2006) Comparison of multiple Amber force fields and development of improved protein backbone parameters. *Proteins* **65**, 712–725
108. Krieger, E., Koraimann, G., and Vriend, G. (2002) Increasing the precision of comparative models with YASARA NOVA—a self-parameterizing force field. *Proteins* **47**, 393–402
109. Jorgensen, W. L., Chandrasekhar, J., Madura, J. D., Impey, R. W., and Klein, M. L. (1983) Comparison of simple potential functions for simulating liquid water. *J. Chem. Phys.* **79**, 926–935
110. Bussi, G., Donadio, D., and Parrinello, M. (2007) Canonical sampling through velocity rescaling. *J. Chem. Phys.* **126**, 014101
111. Parrinello, M., and Rahman, A. (1981) Polymorphic transitions in single crystals: a new molecular dynamics method. *J. Appl. Phys.* **52**, 7182–7190
112. Hess, B., Bekker, H., Berendsen, H. J. C., and Fraaije, J. G. E. M. (1997) Lincs: a linear constraint solver for molecular simulations. *J. Comput. Chem.* **18**, 1463–1472
113. Essmann, U., Perera, L., Berkowitz, M. L., Darden, T., Lee, H., and Pedersen, L. G. (1995) A smooth particle mesh Ewald method. *J. Chem. Phys.* **103**, 8577–8593
114. William, H., Andrew, D., and Klaus, S. (1996) Vmd: visual molecular dynamics. *J. Mol. Graph.* **14**, 33–38